10212–10229 *Nucleic Acids Research, 2022, Vol. 50, No. 18* *Published online 26 September 2022*
https://doi.org/10.1093/nar/gkac777

Thermal stabilisation of the short DNA duplexes by acridine-4-carboxamide derivatives

Filip Kostelansky[1,*], Miroslav Miletin[1], Zuzana Havlinova[2], Barbora Szotakova[2], Antonin Libra[2], Radim Kucera[1], Veronika Novakova[1] and Petr Zimcik[1,*]

[1]Faculty of Pharmacy in Hradec Králové, Charles University, Ak. Heyrovskeho 1203, Hradec Kralove, 500 05, Czech Republic and [2]Generi Biotech, Machkova 587, Hradec Kralove, 500 11, Czech Republic

Received December 09, 2021; Revised August 17, 2022; Editorial Decision August 17, 2022; Accepted August 29, 2022

ABSTRACT

The short oligodeoxynucleotide (ODN) probes are suitable for good discrimination of point mutations. However, the probes suffer from low melting temperatures. In this work, the strategy of using acridine-4-carboxamide intercalators to improve thermal stabilisation is investigated. The study of large series of acridines revealed that optimal stabilisation is achieved upon decoration of acridine by secondary carboxamide carrying sterically not demanding basic function bound through a two-carbon linker. Two highly active intercalators were attached to short probes (13 or 18 bases; designed as a part of HFE gene) by click chemistry into positions 7 and/or 13 and proved to increase the melting temperate (T_m) of the duplex by almost 8°C for the best combination. The acridines interact with both single- and double-stranded DNAs with substantially preferred interaction for the latter. The study of interaction suggested higher affinity of the acridines toward the GC- than AT-rich sequences. Good discrimination of two point mutations was shown in practical application with HFE gene (wild type, H63D C > G and S65C A > C mutations). Acridine itself can also serve as a fluorophore and also allows discrimination of the fully matched sequences from those with point mutations in probes labelled only with acridine.

GRAPHICAL ABSTRACT

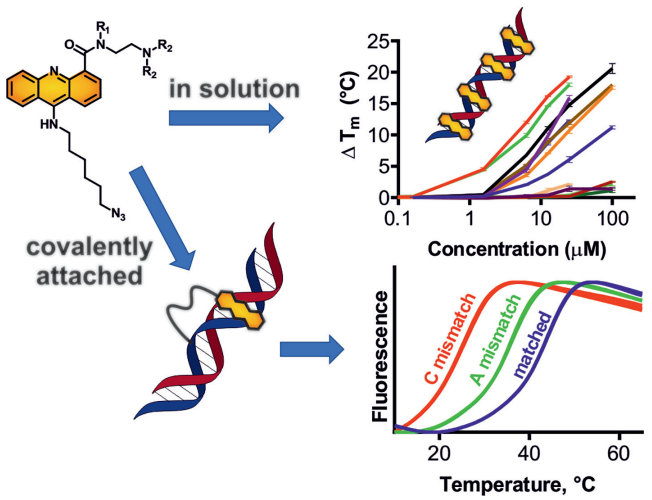

INTRODUCTION

Fluorescent hybridisation probes are invaluable tool for detection of specific oligonucleotide sequences in homogenous solutions (1,2). Since the invention of the polymerase chain reaction (PCR), an extensive effort has been made to develop fluorescent hybridisation probes able to discriminate point mutations or single nucleotide polymorphisms. The length of the fluorescent hybridisation oligonucleotide probe has a crucial role in the mismatch discrimination ability of the probe—in particular, short probes have advantageous properties. However, the short probes suffer from low melting temperatures and the use of agents thermally stabilising the duplex is mostly unavoidable. Different types of stabilising agents have been described with minor groove binders (3,4), polyamines (5,6) and intercalators (7–10) being the most promising. Among these agents, acridine derivatives representing the last group, have been demonstrated to be the promising structural motifs thanks to their strong interaction with DNA. Specifically, 9-amino-6-chloro-2-methoxyacridine (11–13) (Figure 1A),

*To whom correspondence should be addressed. Tel: +420 495067257; Email: zimcik@faf.cuni.cz
Correspondence may also be addressed to Filip Kostelansky. Email: kostelaf@faf.cuni.cz

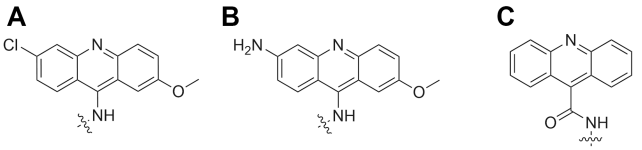

Figure 1. Published acridine derivatives used for modification of DNA.

6,9-diamino-2-methoxyacridine (14,15) (Figure 1B) and acridine-9-carboxamide derivatives (16) (Figure 1C) have been conjugated with oligo(deoxy)nucleotides either during synthesis of oligodeoxynucleotide (ODN) (11,12,17–20) or as a postsynthetic modification (16,21–23) of the ODN, and prepared conjugates have been studied for their ability to influence properties of DNA.

A lot of effort has also been put into the investigation of biological activity and intercalation (24–27) of acridine derivatives for application in anticancer (28–31), antimicrobial (32) or antiviral therapy (33). Disclosed structure–activity relationships emphasize the high binding affinity of acridine-4-carboxamide derivatives toward duplex DNA (29–31,34,35). Their mechanism of biological action was confirmed to be based mainly on their intercalation, followed by inhibition of topoisomerase (36,37). Interaction of acridine derivatives with DNA is, however, complex and includes more processes (38). Presence of ionizable amino moiety in the side chain seems to be advantageous since it helps to 'anchor' the acridine after intercalation (39,40). Early studies confirmed that the intercalation of acridine is not precluded after its covalent binding to a sequence of ODN (11,20,41–43). Considering all these data, we hypothesized that the use of acridine-4-carboxamides covalently attached to ODN may help in thermal stabilisation of the duplex and increase selectivity of the short ODN probes. In this work, we present deep investigation of the series of acridines from the point of view of their structure and their effect on the thermal stabilisation of DNA duplex either freely in the solution or after their attachment to the ODN probe. The ability of the acridines to help in discrimination of single mismatched mutations was tested.

Considering the modification of the ODN molecule by the selected label, several ways to attach a functional molecule to a synthetic ODN exist. It can be incorporated during synthesis of ODN in the synthesizer employing corresponding building blocks, usually phosphoramidites. Alternatively, post-synthetic labelling can be employed, either on the ODN still bound on the solid support or after its cleavage from the solid support and deprotection (in solution). The first approach brings advantage of easier purification by simple washing off the unreacted material and higher stability of the oligonucleotide chain, which is still protected. In addition, the reaction can be performed in a wide spectrum of solvents and water solubility of the label is not crucial. Thus, even highly lipophilic molecules can be attached to the oligonucleotide. Lower consumption of the label can be considered as another great advantage of this approach. The only disadvantage is the reduced accessibility of the reactive moiety on the solid support bounding ODN requiring more efficient and straightforward reaction types. That is why, copper-free ring-strain promoted azide-alkyne cycloaddition has become the most popular reaction due to its high efficiency, selectivity, and simple reaction procedure (44–48). Therefore, we have decided to use it in this project.

MATERIALS AND METHODS

General

All organic solvents used in the synthesis were of analytical grade. Phenol used as solvent for reaction was purified by distillation. All other chemicals for the syntheses were purchased from certified suppliers (i.e. TCI Europe, Acros, Fluorochem, and Merck) and used as received. TLC was performed on Merck aluminium sheets coated with silica gel 60 F254. Merck Kieselgel 60 (0.040–0.063 mm) was used for column chromatography. The ^{1}H and ^{13}C NMR spectra were recorded on a Varian VNMR S500 NMR spectrometer (Varian, Palo Alto, CA, USA) and Jeol JNM-ECZ600R spectrometer (Jeol, Peabody, MA, USA). The chemical shifts are reported as δ values in ppm and are indirectly referenced to Si $(CH_3)_4$ *via* the signal from the solvent. *J* values are given in Hz. The UV/Vis spectra were recorded using a Shimadzu UV-2600 spectrophotometer (Kyoto, Japan). Fluorescence spectra were measured using FLS1000 spectrofluorometer (Edinburgh Instruments, Edinburgh, UK). HRMS spectra were measured using an UHPLC system Acquity UPLC I-class (Waters, Millford, USA) coupled to a high resolution mass spectrometer (HRMS) Synapt G2Si (Waters, Manchester, UK) based on Q-TOF. Chromatographic separations were performed on a Shimadzu LC20 chromatograph (Kyoto, Japan), composed of a DGU-20A3 solvent degasser, two LC-20AD binary gradient pumps, a SIL-20AC autosampler with a 100-μl sample loop, a CTO-20AC column oven, a SPD-M20A photodiode array detector (PDA) and a CBM-20A system controller. The chromatographic data were recorded and analyzed by LabSolutions software 5.3 (Shimadzu, Kyoto, Japan). Semipreparative HPLC was carried out using a Phenomenex Luna 5u Phenyl-Hexyl (150 × 3.0 mm; particle size 5 μm) column using isocratic elution with acetonitrile (ACN) and 50 mmol triethylammonium acetate buffer at flow-rate 1 ml/min and 40°C. Mass spectra of the oligonucleotide probes were obtained using a MALDI-TOF Bruker Daltonics Autoflex II mass spectrometer (Bruker, Bellerica, MA, USA) with 3-hydroxypicolinic acid and ammonium citrate in 50% acetonitrile as a matrix.

The following amines were prepared according to published procedures: *tert*-butyl (2-aminoethyl)carbamate (49), 1,6-diazidohexane (50), 6-azidohexane-1-amine (50) and bis (2-methyl-2-propanyl) {[(2-aminoethyl)amino]methylidene}biscarbamate (51).

Synthesis

Preparation of N- (6-azidohexyl)acridin-9-amine (**1**). The mixture of **13** (1.00 g, 4.7 mmol) and phosphorus oxychloride (10 ml) was stirred at 140°C for 1 h. Then, the excess of phosphorus oxychloride was evaporated under reduced pressure. The crude product was used without further purification in next reaction. Dry phenol (4.42 g, 47 mmol) was added, and the mixture was stirred at 110°C

for 15 min. The 6-azidohexane-1-amine (1.34 g, 9.41 mmol) was added to the mixture cooled to 55°C and the mixture was stirred for 24 h. The reaction mixture was dissolved in chloroform and washed with 2 M sodium hydroxide (50 ml). The organic layer was separated, dried over sodium sulphate, and evaporated under reduced pressure. The product was purified by column chromatography on silica (ethyl acetate). Pure fractions were collected and evaporated under reduced pressure; 282 mg of yellow crystals were obtained. MP: 100.6–102.2°C. Yield 19%. ^{1}H NMR (500 MHz, $CDCl_3$) δ 10.21 (bs, 1H); 8.45 (d, J = 8.6 Hz, 2H); 8.07 (d, J = 8.5 Hz, 2H); 7.48 (t, J = 7.7 Hz, 2H); 7.21 (t, J = 7.8 Hz, 2H); 4.06 (t, J = 7.5 Hz, 2H); 3.18 (t, J = 6.8 Hz, 2H); 2.04 (p, J = 7.5 Hz, 2H); 1.56–1.33 (m, 6H); ^{13}C NMR (126 MHz, $CDCl_3$) δ 156.62; 140.30; 138.58; 125.22; 122.93; 119.68; 112.49; 51.07; 48.58; 29.81; 28.51; 26.29; 26.19. IR (ATR) ν_{max} = 3188, 3030, 2934, 2859, 2788, 2094, 1635, 1588, 1569, 1535, 1473, 1362, 1340, 1272, 1191, 1170, 1143, 1115, 1091, 1036, 953, 869, 748, 733, 698, 661, 640, 632 cm^{-1}. HRMS (m/z): $[M+H]^+$ calcd for $C_{19}H_{22}N_5$, 320.1870, found, 320.1879.

General procedure for preparation of amides **2–12.** Acid **17** (200 mg, 0.55 mmol) was dissolved in $SOCl_2$ (2 ml), and the mixture was stirred at room temperature for 1 h. $SOCl_2$ was then evaporated under reduced pressure. The residue was dissolved in dry dichloromethane (DCM) and added dropwise to ice-cold stirred solution of corresponding amine (1 eq.), and triethylamine (4 eq.) in dry DCM. The reaction mixture was stirred for 30 min. DCM was evaporated from the reaction mixture under reduced pressure. The product was purified by column chromatography on silica. After purification and characterization, the free amines were converted to the corresponding hydrochlorides that were more stable. The acridines were dissolved in diethyl ether (50 ml) and bubbled by HCl gas generated from NaCl and H_2SO_4. The hydrochlorides then separated as an oily yellow liquid. The diethyl ether was decanted and the oily residue was washed 3 times with diethyl ether (50 ml), dissolved in MeOH, and evaporated to dryness. The amount of HCl in the sample was determined by titration with $AgNO_3$ (see Supplementary Data, Figure S1).

Preparation of 9-[(6-azidohexyl)amino]-N-[2-(dimethylamino)ethyl]acridine-4-carboxamide (**2**). This compound was prepared using the General procedure above. Mobile phase–ethyl acetate:MeOH:TEA 95:5:1, R_f = 0.19. Yellow oil, 60%. Data for free base: ^{1}H NMR (600 MHz, acetone-d_6) δ 12.43 (s, 1H); 8.72 (s, 1H); 8.50 (d, J = 8.7, 1.6 Hz, 1H); 8.38 (d, J = 8.6 Hz, 1H); 8.04 (s, 1H); 7.71 (t, J = 7.0 Hz, 1H); 7.47–7.30 (m, 2H); 6.81 (bs, 1H); 3.91 (t, J = 7.2 Hz, 2H); 3.65 (q, J = 5.8 Hz, 2H); 3.22 (t, J = 6.9 Hz, 2H); 2.61 (t, J = 6.1 Hz, 2H); 2.36 (s, 6H); 1.84 (p, J = 7.4 Hz, 2H); 1.50 (p, J = 7.0 Hz, 2H); 1.45–1.30 (m, 4H); ^{13}C NMR (151 MHz, acetone-d_6) δ 165.66; 153.42; 148.12; 147.29; 133.98; 130.64; 129.15; 128.45; 127.64; 123.73; 122.87; 121.19; 116.54; 115.63; 58.44; 51.03; 50.53; 44.83; 37.53; 30.87; 28.54; 26.28; 26.25. IR (ATR) ν_{max} = 3369, 2940, 2860, 2817, 2767, 2086, 1748, 1714, 1680, 1643, 1617, 1594, 1558, 1532, 1503, 1475, 1457, 1441, 1429, 1373, 1355, 1326, 1292, 1272, 1255, 1212, 1187, 1149, 1130, 1072, 1057, 1042, 941, 918, 884, 849, 780, 763, 748, 736, 681, 656,643, 632, 617 cm^{-1}. HRMS (m/z): $[M+H]^+$ calcd for $C_{24}H_{32}N_7O$, 434.2663, found, 434.2670.

Preparation of tert-butyl (2-{9-[(6-azidohexyl)amino]acridine-4-carboxamido}ethyl)carbamate (**3-Boc**). This compound was prepared using the General procedure above but without the final conversion to hydrochloride. Mobile phase–ethyl acetate:MeOH:TEA, R_f = 0.46. Yellow oil, 63%. ^{1}H NMR (600 MHz, $CDCl_3$) δ 12.51 (s, 1H), 8.80 (s, 1H), 8.17 (d, J = 8.7 Hz, 1H), 8.06 (d, J = 8.7 Hz, 1H), 7.97 (s, 1H), 7.67 (t, J = 7.8 Hz, 1H), 7.37 (s, 2H), 5.51–5.14 (m, 2H), 3.85–3.69 (m, 4H), 3.49 (q, J = 5.8 Hz, 2H), 3.21 (t, J = 6.8 Hz, 2H), 1.77 (p, J = 7.2 Hz, 2H), 1.55 (p, J = 7.0 Hz, 2H), 1.49–1.35 (m, 13H). ^{13}C NMR (151 MHz, $CDCl_3$) δ 167.34, 156.30, 152.74, 147.89, 147.25, 134.80, 130.83, 129.63, 127.99, 126.86, 123.66, 122.49, 122.07, 116.54, 115.76, 79.32, 51.31, 51.04, 41.29, 39.63, 31.69, 28.76, 28.55, 26.50. IR (ATR) ν_{max} = 3370, 2932, 2860, 2098, 1678, 1639, 1620, 1557, 1524, 1459, 1435, 1391, 1364, 1351, 1270, 1252, 1166, 1147, 1129, 1093, 1064, 1046, 1022, 847, 749, 730, 716, 683, 653, 642, 635, 627, 621, 609, 605 cm^{-1}. HRMS (m/z): $[M + H]^+$ calcd for $C_{27}H_{36}N_7O_3$, 506.2874, found, 506.2873.

Preparation of N-(2-aminoethyl)-9-[(6-azidohexyl)amino]acridine-4-carboxamide (**3**). Compound **3-Boc** (202 mg, 0.4 mmol) was dissolved in DCM (3 ml). Trifluoroacetic acid (TFA) (2.98 g, 26 mmol) was added to the stirring solution. The mixture was stirred for 1 h at room temperature and monitored by TLC. The solvents were then evaporated under reduced pressure. The product was purified by column chromatography on silica ($CHCl_3$:MeOH 4:1, R_f = 0.21). Pure fractions were collected and evaporated. The product was dissolved in $CHCl_3$ (25 ml) and washed with 1M NaOH (25 ml) three times. Organic layer was collected, dried over sodium sulphate, and evaporated. Dark yellow oil (80 mg) was obtained and converted to dihydrochloride according to general procedure. Yield (42%). Data for dihydrochloride: ^{1}H NMR (500 MHz, CD_3OD) δ 8.69 (bs, 1H); 8.55 (d, J = 7.4 Hz, 1H); 8.52–8.40 (bs, 1H); 7.98 (t, J = 7.7 Hz, 1H); 7.84 (d, J = 8.4 Hz, 1H); 7.67–7.52 (m, 2H); 4.14 (t, J = 7.5 Hz, 2H); 3.83 (t, J = 5.8 Hz, 2H); 3.33–3.25 (m, 2H); 2.02 (p, J = 7.1 Hz, 2H); 1.61 (p, J = 6.7 Hz, 2H); 1.57–1.42 (m, 4H); ^{13}C NMR (126 MHz, CD_3OD) δ 170.39; 159.92; 136.95; 136.23; 128.76; 126.08; 120.43; 119.68; 114.99; 52.29; 50.67; 40.92; 38.74; 30.33; 29.69; 27.34; 27.32. IR (ATR) ν_{max} = 2930, 2861, 2095, 1643, 1621, 1590, 1566, 1535, 1478, 1443, 1351, 1310, 1273, 1251, 1178, 1132, 1073, 1037, 898, 842, 823, 755,659, 649,640, 633, 626, 614, 602 cm^{-1}. HRMS (m/z): $[M + H–2HCl]^+$ calcd for $C_{22}H_{28}N_7O$, 406.2350, found, 406.2352.

Preparation of bis (2-methyl-2-propanyl){[(2-{9-[(6-azidohexyl)amino]acridine-4-carboxamido}ethyl)amino]methylylidene}biscarbamate (**4-Boc**). This compound was prepared using the General procedure above but without the final conversion to hydrochloride. Mobile phase ethyl acetate:MeOH:TEA 100:1:0.5 R_f = 0.47. Yellow oil, 88%. ^{1}H NMR (600 MHz, acetone-d_6) δ 12.50–12.40 (m, 1H); 11.65 (s, 1H); 8.76–8.71 (m, 1H); 8.61–8.55 (m, 1H); 8.54–8.50 (m, 1H); 8.39 (d, J = 8.7 Hz, 1H); 7.98 (d, J = 8.6 Hz, 1H); 7.73–7.66 (m,

1H); 7.44–7.36 (m, 2H); 6.82–6.74 (m, 1H); 3.95 (q, $J = 7.4$ Hz, 2H); 3.85–3.79 (m, 2H); 3.76 (q, $J = 5.8$ Hz, 2H); 3.25 (t, $J = 6.9$ Hz, 2H); 1.93–1.82 (m, 2H); 1.57–1.33 (m, 24H); ^{13}C NMR (151 MHz, acetone-d_6) δ 166.21; 163.85; 156.49; 153.62; 152.84; 148.16; 147.41; 134.34; 130.78; 129.28; 128.24; 127.74; 123.60; 122.96; 121.23; 116.43; 115.54; 82.68; 77.97; 51.02; 50.52; 50.41; 40.99; 40.87; 38.48; 38.36; 30.81; 29.51; 28.52; 27.64; 27.23; 26.23. IR (ATR) ν_{max} = 2932, 2859, 2095, 1721, 1639 1618, 1560, 1526, 1510, 1457, 1413, 1393, 1367, 1351, 1328, 1278, 1253, 1229, 1156, 1134, 1051, 1024, 879, 853, 809, 759, 737, 702, 678, 657 cm^{-1}. HRMS (m/z): [M + H]$^+$ calcd for $C_{33}H_{46}N_9O_5$, 648.3616, found, 648.3621.

*Preparation of 9-[(6-azidohexyl)amino]-N-(2-guanidinoethyl)acridine-4-carboxamide (**4**).* Compound **4-Boc** (150 mg, 0.23 mmol) was dissolved in DCM (3 ml). TFA (2.98 g, 26 mmol) was added to the stirring solution. The mixture was stirred for 2 h at room temperature and monitored by TLC. The solvents were then evaporated under reduced pressure. The product was purified by column chromatography on silica ($CHCl_3$:MeOH 4:1, $R_f = 0.20$). Pure fractions were collected and evaporated. The product was dissolved in $CHCl_3$ (25 ml) and washed three times with 1M NaOH (25 ml). The organic layer was collected, dried over sodium sulphate, and evaporated. Dark yellow oil (62 mg) was obtained. The compound was then converted to the dihydrochloride according to general procedure. Yield 48%. Data for dihydrochloride: ^{1}H NMR (500 MHz, CD_3OD) δ 8.46–8.27 (m, 2H); 8.19 (bs, 1H); 7.87–7.55 (m, 2H); 7.36 (bs, 2H); 3.84 (bs, 2H); 3.66 (t, $J = 6.4$ Hz, 2H); 3.53 (t, $J = 6.4$ Hz, 2H); 3.21 (t, $J = 6.8$ Hz, 2H); 1.83 (bs, 2H); 1.53 (p, $J = 6.8$ Hz, 2H); 1.37 (bs, 4H). ^{13}C NMR (126 MHz, CD_3OD) δ 168.37, 157.72, 134.41, 129.02, 123.61, 121.51, 51.02, 49.43, 48.58, 40.75, 38.62, 29.58, 28.43, 26.07. IR (ATR) ν_{max} = 3129, 2928, 2857, 2095, 1668, 1642, 1620, 1563, 1462, 1352, 1308, 1273, 1252, 1178, 1129, 900, 858, 757,728, 677, 659, 631, 621, 609. HRMS (m/z): [M+H]$^+$ calcd for $C_{23}H_{30}N_9O$, 448.2568, found, 448.2572.

Preparation of 9-[(6-azidohexyl)amino]-N-[3-(dimethylamino)propyl]acridine-4-carboxamide (**5**). This compound was prepared using the General procedure above. Mobile phase: ethyl acetate:MeOH:TEA 95:5:1, $R_f = 0.1$. Data for free base: ^{1}H NMR (600 MHz, acetone-D_6) δ 12.32 (s, 1H), 8.74 (s, 1H), 8.48 (d, $J = 8.6$ Hz, 1H), 8.36 (d, $J = 8.7$ Hz, 1H), 7.95 (bs, 1H), 7.75–7.61 (m, 1H), 7.46–7.25 (m, 2H), 6.85 (bs, 1H), 3.88 (t, $J = 7.2$ Hz, 2H), 3.61 (q, $J = 6.6$ Hz, 2H), 3.19 (t, $J = 6.9$ Hz, 2H), 2.43 (t, $J = 7.1$ Hz, 2H), 2.18 (s, 6H), 1.87 (p, $J = 6.9$ Hz, 2H), 1.81 (p, $J = 7.2$ Hz, 2H), 1.47 (p, $J = 7.0$ Hz, 2H), 1.41–1.27 (m, 4H). ^{13}C NMR (151 MHz, acetone-D_6) δ 165.84, 153.52, 148.12, 147.43, 134.19, 130.77, 128.98, 128.38, 127.72, 123.85, 122.84, 121.14, 116.46, 115.54, 57.53, 51.03, 50.53, 45.05, 37.57, 30.90, 28.56, 27.84, 26.31, 26.27. IR (ATR) ν_{max} 3228, 2938, 2686, 2096, 1621, 158, 1567, 1537, 1476, 1443, 1349, 1311, 1273, 1248, 1177, 1133, 1091, 1035, 1004, 979, 753, 659, 643, 633, 609 cm^{-1}. HRMS (m/z): [M+H]$^+$ calcd for $C_{25}H_{34}N_7O$, 448.2819, found, 448.2827.

Preparation of 9-[(6-azidohexyl)amino]-N-[2-(pyrrolidin-1-yl)ethyl]acridine-4-carboxamide (**6**). This compound was prepared using the General procedure above. Mobile phase: ethyl acetate:MeOH:TEA 95:5:1 R_f = 0.08. Data from free base: ^{1}H NMR (600 MHz, acetone-D_6) δ 12.47 (s, 1H), 8.74 (d, $J = 7.0$ Hz, 1H), 8.50 (d, $J = 8.8$ Hz, 1H), 8.38 (d, $J = 8.9$ Hz, 1H), 8.09 (d, $J = 8.6$ Hz, 1H), 7.71 (t, $J = 7.6$ Hz, 1H), 7.54 (s, 0H), 7.46–7.30 (m, 2H), 6.76 (s, 1H), 3.97–3.88 (m, 2H), 3.66 (q, $J = 5.7$ Hz, 2H), 3.23 (t, $J = 6.9$ Hz, 2H), 2.77 (t, $J = 6.0$ Hz, 2H), 2.69–2.59 (m, 4H), 1.90–1.78 (m, 6H), 1.52 (p, $J = 7.0$ Hz, 2H), 1.47–1.30 (m, 4H). ^{13}C NMR (151 MHz, acetone-D_6) δ 165.50, 153.43, 148.28, 147.41, 134.10, 130.41, 129.31, 128.72, 127.45, 123.63, 122.95, 121.31, 116.48, 115.54, 55.27, 54.13, 53.86, 51.02, 50.49, 38.72, 30.83, 29.52, 28.53, 26.25, 23.53. IR (ATR) ν_{max} 3391, 3230, 2938, 2614, 2095, 1644, 1622, 1590, 1568, 1537, 1475, 1445, 1401, 1350, 1311, 1272, 1250, 1193, 1178, 1120, 1080, 1015, 899, 821, 755, 659, 641, 633, 625, 617, 610 cm^{-1}. HRMS (m/z): [M+H]$^+$ calcd for $C_{26}H_{34}N_7O$, 460.2819, found, 460.2823.

*Preparation of 9-[(6-azidohexyl)amino]-N-[2-(diethylamino)ethyl]acridine-4-carboxamide (**7**).* This compound was prepared using the General procedure above. Mobile phase: ethyl acetate:MeOH:TEA 95:5:1, R_f = 0.12. Data for free base: ^{1}H NMR (600 MHz, acetone-D_6) δ 12.36–12.29 (m, 1H); 8.79–8.71 (m, 1H); 8.43–8.38 (m, 1H); 8.30–8.25 (m, 1H); 8.12–8.07 (m, 1H); 7.75–7.66 (m, 1H); 7.43–7.33 (m, 2H); 7.25–7. 17 (m, 1H); 3.99–3.88 (m, 2H); 3.63 (q, $J = 6.0$ Hz, 2H); 2.80 (t, $J = 6.0$ Hz, 2H); 2.72 (t, $J = 6.2$ Hz, 2H); 2.67 (q, $J = 7.0$ Hz, 1H); 2.62 (q, $J = 7.0$ Hz, 1H); 1.10–0.98 (m, 12H). ^{13}C NMR (151 MHz, acetone-D_6) δ 165.51, 153.11, 148.22, 147.46, 134.15, 130.47, 129.39, 128.74, 127.19, 123.36, 122.81, 121.14, 116.09, 115.17, 52.38, 52.31, 51.02, 50.51, 46.97, 46.55, 46.11, 37.81, 30.85, 26.26, 11.58, 11.50. IR (ATR) ν_{max} 3391, 3233, 2980, 2649, 2486, 2097, 1622, 1588, 1569, 1537, 1474, 1397, 1352, 1313, 1273, 1247, 1180, 1141, 1015, 968, 755, 660, 651, 633, 606 cm^{-1}. HRMS (m/z): [M + H]$^+$ calcd for $C_{26}H_{36}N_7O$, 462.2976, found, 462.2977.

*Preparation of 9-[(6-azidohexyl)amino]-N-[2-(piperidin-1-yl)ethyl]acridine-4-carboxamide (**8**).* This compound was prepared using the General procedure above. Mobile phase: ethyl acetate:MeOH:TEA 95:5:1. $R_f = 0.2$. Data for free base: ^{1}H NMR (600 MHz, acetone-d_6) δ 12.30 (s, 1H), 8.74 (d, $J = 7.4$ Hz, 1H), 8.51 (d, $J = 8.8$ Hz, 1H), 8.39 (d, $J = 8.8$ Hz, 1H), 8.19 (d, $J = 8.7$ Hz, 1H), 7.72 (t, $J = 7.6$ Hz, 1H), 7.47–7.32 (m, 2H), 6.76 (s, 1H), 3.94 (q, $J = 6.9$ Hz, 2H), 3.66 (q, $J = 5.8$ Hz, 2H), 3.24 (t, $J = 6.9$ Hz, 2H), 2.62 (t, $J = 6.2$ Hz, 2H), 2.51 (bs, 4H), 1.86 (p, $J = 7.3$ Hz, 2H), 1.64 (p, $J = 5.7$ Hz, 4H), 1.53 (p, $J = 7.0$ Hz, 2H), 1.50–1.41 (m, 4H), 1.41–1.32 (m, 2H). ^{13}C NMR (151 MHz, acetone-d_6) δ 165.50; 153.46; 148.24; 147.44; 134.16; 130.43; 129.56; 128.68; 127.47; 123.64; 122.97; 121.31; 116.47; 115.54; 58.42; 54.61; 51.02; 50.50; 50.38; 36.96; 36.85; 30.80; 28.52; 26.24; 26.03; 24.53. IR (ATR) ν_{max} 3226,2941, 2862, 2648, 2541, 2095, 1622, 1590, 1568, 1537, 1474, 1443, 1350, 1310, 1272, 1179, 1134, 1099, 1037, 1007, 949, 897, 856, 755, 659, 632, 624, 609 cm^{-1}. HRMS (m/z): [M+H]$^+$ calcd for $C_{27}H_{36}N_7O$, 474.2976, found, 474.2974.

Preparation of 9-[(6-azidohexyl)amino]-N-butylacridine-4-carboxamide (**9**). This compound was prepared using the General procedure above but without the final conversion to hydrochloride. Mobile phase ethyl

acetate:MeOH:TEA 96:2:2, R_f = 0.54. Yellow oil, 59%. Data for free base: ^{1}H NMR (600 MHz, acetone-d_6) δ 12.23 (s, 1H); 8.74 (s, 1H); 8.50 (d, J = 8.7 Hz, 1H); 8.39 (d, J = 8.8 Hz, 1H); 7.95 (d, J = 8.5 Hz, 1H); 7.72 (t, J = 7.6 Hz, 1H); 7.39 (p, J = 6.1 Hz, 2H); 6.80 (s, 1H); 3.93 (t, J = 7.0 Hz, 2H); 3.57 (q, J = 6.5 Hz, 2H); 3.23 (t, J = 7.0 Hz, 2H); 1.86 (p, J = 7.4 Hz, 2H); 1.72 (p, J = 7.0 Hz, 2H); 1.61–1.47 (m, 4H); 1.47–1.31 (m, 4H); 1.00 (t, J = 7.4 Hz, 3H); ^{13}C NMR (151 MHz, acetone-d_6) δ 165.5; 153.63; 148.16; 147.49; 134.24; 130.87; 128.93; 128.56; 127.52; 123.75; 122.93; 121.27; 116.44; 115.52; 51.01; 50.51; 38.93; 31.83; 30.81; 28.52; 26.23; 20.40; 13.33. IR (ATR) ν_{max} = 3358, 2932, 2861, 2095, 1639, 1617, 1593, 1560, 1532, 1503, 1476, 1435, 1423, 1371, 1357, 1328, 1273, 1254, 1211, 1187, 1149, 1127, 1094, 1027, 956, 918, 848, 822, 763, 746, 736, 680, 657, 630, 617 cm^{-1}. HRMS (m/z): [M+H]$^+$ calcd for $C_{24}H_{31}N_6O$, 419.2554, found, 419.2562.

Preparation of 9-[(6-azidohexyl)amino]-N-[2-(dimethylamino)ethyl]-N-methylacridine-4-carboxamide (**10**). This compound was prepared using the General procedure above. Mobile phase: ethyl acetate:MeOH:TEA 95:5:1. R_f = 0.1. Data for free base: ^{1}H NMR (500 MHz, CD_3OD) δ 8.36 (t, J = 10.0 Hz, 1H); 8.28 (t, J = 9.0 Hz, 1H); 7.99 (d, J = 8.9 Hz, 1H); 7.94 (d, J = 8.8 Hz, 1H); 7.69–7.60 (m, 2H); 7.36 (p, J = 8.3 Hz, 2H); 3.87 (bs, 1H); 3.83 (q, J = 6.8 Hz, 2H); 3.27 (s, 1.5H); 3.23 (t, J = 7.7 Hz, 1H); 3.22–3.14 (m, 2H); 2.85–2.77 (m, 2.5H); 2.54 (t, J = 7.7 Hz, 1H); 2.42 (s, 3H); 1.84 (s, 3H); 1.76 (p, J = 7.3 Hz, 2H); 1.54–1.44 (m, 2H); 1.37–1.29 (m, 4H). ^{13}C NMR (126 MHz, CD_3OD) δ 172.24, 152.76, 152.63, 130.19, 130.01, 128.14, 127.83, 125.00, 123.45, 122.55, 121.17, 121.07, 116.25, 56.50, 55.48, 50.88, 49.89, 44.88, 44.41, 43.92, 36.21, 32.12, 30.59, 30.54, 28.34, 26.06, 26.04. IR (ATR) ν_{max} 2936, 2095, 1629, 1592, 1573, 1538, 1446, 1404, 1351, 1293, 1269, 1168, 1149, 1104, 1088, 1041, 976, 898, 857, 817, 759, 687, 656, 647, 637, 605 cm^{-1}. HRMS (m/z): [M + H]$^+$ calcd for $C_{25}H_{34}N_7O$, 448.2819, found, 448.2823.

Preparation of (9-((6-azidohexyl)amino)acridin-4-yl)(4-methylpiperazin-1-yl)methanone (**11**). This compound was prepared using the General procedure above. Mobile phase: ethyl acetate:MeOH:TEA 95:5:1, R_f = 0.1. Data for free base: ^{1}H NMR (600 MHz, acetone-d_6) δ 8.40–8.31 (m, 2H); 7.93–7.89 (m, 1H); 7.67–7.61 (m, 1H); 7.56–7.52 (m, 1H); 7.37–7.31 (m, 2H); 6.47–6.38 (m, 1H); 3.95–3.85 (m, 3H); 3.75 (m, 1H); 3.25 (t, J = 6.9 Hz, 2H); 3.16–3.10 (m, 1H); 3.07–3.01 (m, 1H); 2.59–2.53 (m, 1H); 2.43–2.33 (m, 2H); 2.20 (s, 3H); 2.08–2.03 (m, 1H); 1.84 (p, J = 7.3 Hz, 2H); 1.53 (p, J = 7.9 Hz, 2H); 1.46–1.40 (m, 2H); 1.40–1.33 (m, 2H); ^{13}C NMR (151 MHz, acetone-D_6) δ 168.57, 151.88, 149.59, 146.46, 137.61, 130.04, 129.74, 127.47, 124.23, 123.60, 122.83, 121.87, 116.61, 116.23, 55.09, 54.84, 51.03, 50.41, 50.30, 46.78, 45.65, 41.29, 30.96, 28.54, 26.28. IR (ATR) ν_{max} 2936,2602, 2095, 1629, 1592, 1573, 1538, 1445, 1351, 1269, 1198, 1165, 1131, 1090, 1023, 974, 902, 860, 816, 758, 681, 656, 647, 628, 613 cm^{-1}. HRMS (m/z): [M + H]$^+$ calcd for $C_{25}H_{32}N_7O$, 446.2663, found, 446.2669.

Preparation of 9-[(6-azidohexyl)amino]-N,N-bis[2-(diethylamino)ethyl]acridine-4-carboxamide (**12**). This compound was prepared using the General procedure above. Mobile phase: ethyl acetate:MeOH:TEA 95:5:1, R_f = 0.07. Data for free base: ^{1}H NMR (500 MHz, CD_3OD) δ 8.39 (d, J = 8.7 Hz, 1H); 8.31 (d, J = 7.7 Hz, 1H); 7.96 (d, J = 8.7 Hz, 1H); 7.71–7.64 (m, 1H); 7.64–7.60 (m, 1H); 7.43–7.35 (m, 2H); 3.86 (t, J = 7.2 Hz, 3H); 3.81 (bs, 2H); 3.27–3.18 (m, 4H); 3.08–2.92 (bs, 2H); 2.74 (q, J = 7.2 Hz, 4H); 2.78–2.70 (bs, 2H); 2.11 (q, J = 7.2 Hz, 4H); 1.78 (p, J = 7.3 Hz, 2H); 1.52 (p, J = 6.9 Hz, 2H); 1.43–1.30 (m, 4H); 1.19 (t, J = 7.2 Hz, 6H); 0.61 (t, J = 7.2 Hz, 6H); ^{13}C NMR (126 MHz, CD_3OD) δ 172.40, 152.54, 134.06, 132.15, 130.02, 128.84, 127.80, 127.66, 125.97, 124.92, 123.33, 122.62, 121.96, 121.12, 120.57, 117.31, 116.38, 50.89, 50.53, 49.90, 49.55, 47.38, 47.10, 46.71, 43.49, 30.56, 28.36, 26.09, 26.06, 10.62, 9.94. IR (ATR) ν_{max} 3411, 2942, 2650, 2482, 2096, 1629, 1593, 1574, 1537, 1464, 1445, 1397, 1352, 1327, 1268, 1197, 1169, 1125, 1070, 1038, 969, 895, 817, 763, 678, 660, 652, 641, 606 cm^{-1}. HRMS (m/z): [M+H]$^+$ calcd for $C_{32}H_{49}N_8O$, 561.4024, found, 561.4030.

Preparation of 2-(phenylamino)benzoic acid (**13**). To solution of 2-chlorobenzoic acid (20.46 g, 131 mmol) in isoamyl alcohol (120 ml) was added catalytic amount of copper powder and potassium carbonate (36.11 g, 261 mmol). Aniline (12.24 g, 131 mmol) was added into the stirring reaction mixture, and the reaction mixture was stirred overnight at 140°C. After completion of reaction, isoamyl alcohol was evaporated from reaction mixture under reduced pressure. Crude product was dissolved in 1 M sodium hydroxide (100 ml) and poured into the hot water (1 l). After cooling, the solution was acidified with concentrated hydrochloric acid. Resulting precipitate was filtered and washed with hot water (0.5 l). Then, the product was recrystalized from hot aqueous ethanol (350 ml). Product was purified twice by column chromatography on silica (first column $CHCl_3$, second column $CHCl_3$:MeOH 4:1). Pale-yellow powder was obtained (11.96 g, 43%). ^{1}H NMR (500 MHz, DMSO) δ 13.07 (s, 1H); 9.63 (s, 1H); 7.90 (dd, J = 8.0, 1.7 Hz, 1H); 7.42–7.31 (m, 3H); 7.27–7.19 (m, 3H); 7.07 (t, J = 7.6, 1.3 Hz, 1H); 6.77 (t, J = 8.1, 7.0, 1.1 Hz, 1H); ^{13}C NMR (126 MHz, DMSO) δ 170.41; 147.46; 140.96; 134.63; 132.34; 129.95; 123.55; 121.85; 117.87; 114.20; 113.01.

Preparation of 2,2'-iminodibenzoic acid (**14**). To a mixture of anthranilic acid (6.8 g, 49.6 mmol), 2-chlorobenzoic acid (7.8 g, 49.8 mmol), dry potassium carbonate (5 g, 36 mmol), and catalytic amount of copper powder was added isoamyl alcohol (70 ml). The reaction mixture was stirred overnight at 140°C. Then, isoamyl alcohol was evaporated under reduced pressure. The crude product was poured into the hot water (1 l). The mixture was stirred for 30 min, and then acidified with concentrated hydrochloric acid. The resulting precipitate was collected by vacuum filtration and washed 3 times with hot water. The product was dissolved in 1 M sodium hydroxide, boiled with charcoal, and filtered. Concentrated hydrochloric acid was added, and the resulting precipitate was collected by vacuum filtration, and washed 3 times with water. The product was recrystalized from hot aqueous ethanol; a pale-yellow product was obtained (5.14 g, 32%). ^{1}H NMR (500 MHz, DMSO) δ 13.01 (s, 2H), 10.83 (s, 1H), 7.91 (dd, J = 8.0, 1.6 Hz, 2H), 7.48–7.38 (m, 4H), 6.94 (ddd, J = 8.1, 6.7, 1.5 Hz, 2H). ^{13}C NMR (126 MHz, DMSO) δ 168.56; 143.76; 133.52; 131.97; 120.15; 117.77; 117.74.

*Preparation of methyl 9-oxo-9,10-dihydroacridine-4-carboxylate (***15**). Phosphorus oxychloride (90 ml) was added to 2,2'-iminodibenzoic acid **14** (7.78 g, 30.24 mmol) and the mixture was stirred at 140°C for 1 h. The reaction mixture was cooled to 50°C, and dry methanol (100 ml) was added dropwise. Resulting crystals were dissolved by addition of phosphorus oxychloride (5 ml) and the reaction mixture was stirred for 12 h at 50°C. Methanol was then evaporated under reduced pressure, and the crystals were collected by vacuum filtration. The crystals were recrystallised from hot methanol. Yellow crystals were obtained (6.11 g, 79%), m.p. 170.8–172.1°C. ^{1}H NMR (500 MHz, $CDCl_3$) δ 11.70 (s, 1H); 8.70 (m, 1H); 8.41 (m, 2H); 7.67 (m, 1H); 7.37 (m, 1H); 7.33–7.18 (m, 2H); 4.00 (s, 3H); ^{13}C NMR (126 MHz, $CDCl_3$) δ 177.74; 168.34; 141.66; 139.98; 136.43; 133.88; 133.87; 127.00; 122.34; 122.29; 121.47; 119.78; 117.48; 113.46; 52.43. IR (ATR) ν_{max} = 3267, 3068, 2947, 1687, 1633, 1615, 1596, 1523, 1483, 1464, 1441, 1418, 1356, 1322, 1281, 1202, 1170, 1139, 1113, 1085, 1072, 1027, 1008, 992, 963, 940, 896, 873, 827, 802, 754, 739, 711, 677 cm^{-1}. HRMS (*m/z*): $[M+H]^+$ calcd for $C_{15}H_{12}NO_3$, 254.0812, found, 254.0818.

Preparation of methyl 9-[(6-azidohexyl)amino]acridine-4-carboxylate (**16**). The mixture of **15** (2.06 g, 8.13 mmol) and thionyl chloride (8 ml) was stirred at 80°C for 1 h. Then, the excess of thionyl chloride was evaporated from the reaction mixture under reduced pressure. Dry phenol (7.75 g, 82.35 mmol) was added to the residue and the stirring mixture was heated to 115°C for 15 min. The 6-azidohexane-1-amine (2.95 g, 20.74 mmol) was added to the mixture precooled to 55°C, and the mixture was stirred for 24 h. The reaction mixture was dissolved in chloroform and washed with 2M sodium hydroxide after completion of reaction. The organic layer was separated, dried over sodium sulphate, and evaporated under reduced pressure. The product was purified by column chromatography on silica (ethyl acetate). Pure fractions were collected and evaporated under reduced pressure. Brown-orange oil was obtained (2.42 g, 94%). ^{1}H NMR (500 MHz, $CDCl_3$) δ 11.08 (bs, 1H); 8.99–7.81 (m, 3H); 7.48 (s, 1H); 7.32–6.98 (m, 3H); 4.05–3.84 (m, 5H); 3.27 (t, J = 7.0 Hz, 2H); 2.01–1.81 (m, 2H); 1.65 (p, J = 7.0 Hz, 2H); 1.59–1.42 (m, 4H); ^{13}C NMR (126 MHz, $CDCl_3$) δ 168.56; 140.51; 133.35; 132.66; 131.26; 129.26; 128.90; 120.35; 117.25; 115.53; 52.71; 52.22; 51.40; 32.30; 28.79; 26.99; 26.57. IR (ATR) ν_{max} = 3280, 2935, 2847, 2818, 2091, 1689, 1608, 1573, 1519, 1487, 1465, 1446, 1436, 1415, 1370, 1321, 1279, 1269, 1254, 1195, 1161, 1141, 1124, 1079, 1068, 1019, 995, 941, 908, 891, 854, 829, 780,766, 754, 746, 731, 684, 665, 657, 612. HRMS (*m/z*): $[M+H]^+$ calcd for $C_{21}H_{24}N_5O_2$, 378.1925, found, 378.1928.

Preparation of 9-[(6-azidohexyl)amino]acridine-4-carboxylic acid (**17**): Compound **16** (5.2 g, 14.3 mmol) was dissolved in THF. Excess (10 ml) of saturated solution of sodium hydroxide in aqueous methanol (MeOH:H_2O 5:1) was added to the stirring solution. The mixture was stirred for 1 h at 50°C. Then, the solvents were evaporated from the reaction mixture under reduced pressure. The residue was adsorbed on silica and washed with ethyl acetate (100 ml) 3 times. Then, the silica was washed with mixture of chloroform and methanol ($CHCl_3$:MeOH 4:1) to elute the pure sodium salt. Solvents were evaporated under reduced pressure and the residue was dissolved in chloroform and washed three times with aqueous 10% HCl (50 ml). The organic layer was collected, dried over sodium sulphate, and evaporated under reduced pressure. Orange solid was obtained (4.28 g, 85%), m.p. 174.0–175.7°C. ^{1}H NMR (500 MHz, $CDCl_3$) δ 11.21 (s, 1H), 8.81 (t, J = 6.5 Hz, 2H), 8.71 (d, J = 8.7 Hz, 1H), 7.74 (t, J = 7.6 Hz, 1H), 7.67 (d, J = 8.4 Hz, 1H), 7.44 (t, J = 7.9 Hz, 1H), 7.38 (t, J = 7.9 Hz, 1H), 4.19 (t, J = 7.5 Hz, 2H), 3.16 (t, J = 6.8 Hz, 2H), 2.13 (p, J = 7.5 Hz, 2H), 1.59–1.46 (m, 4H), 1.46–1.36 (m, 2H) ^{13}C NMR (126 MHz, $CDCl_3$) δ 170.69; 158.10; 141.50; 139.48; 137.48; 134.16; 128.46; 126.19; 123.91; 123.05; 122.23; 119.70; 113.45; 112.87; 51.19; 49.20; 29.61; 28.60; 26.49; 26.30. IR (ATR) ν_{max} = 2936, 2859, 2095, 1622, 1584, 1553, 1532, 1479, 1441, 1382, 1337, 1277, 1236, 1171, 1085, 1070, 1041, 972, 935, 889, 780, 750, 663, 642, 632, 619 cm^{-1}. HRMS (*m/z*): $[M+H]^+$ calcd for $C_{20}H_{22}N_5O_2$, 364.1768, found, 364.1779.

Preparation of modified probes

The tested ODNs were prepared by standard phosphoramidite synthesis in DNA/RNA synthesizer (ABI 394 DNA/RNA synthesizer) using ultra-mild protection on the controlled pore glass solid phase support (loading: 30–40 μmol/g). Dibenzoazacyclooctyne (DBCO)-modified thymidine phosphoramidite (with a seventeen atoms-long linker, for structure see Supplementary Figure S2) was introduced into selected positions during the synthesis. To 4 mg of the prepared support in a 2.5-ml plastic vial was added 200 μl of solution of corresponding modifier in methanol (approximately 50 mM concentration). The mixture was agitated 24 h in the dark. Then, the solution and the support were separated, and the support was washed with pure methanol (500 μl) 5 times. Then, 0.05 M K_2CO_3 in methanol (500 μl) was added to the support, and the mixture was agitated in the dark for 8 h. Water (500 μl) was added to the mixture, so the combined volume was equal to 1 ml. Deprotected modified probes were prepurified by size-exclusion filtration columns (CentriPure N10, emp Biotech GmbH, Berlin, Germany). The whole volume (1 ml) was transferred to the gel chromatography column and the volume was allowed to enter the gel bed completely. Then, 1.5 ml of purified water was transferred to the column, and the modified probe was eluted to the vial. The solution of the modified probe was evaporated under reduced pressure, and the residue was dissolved in purified water (120 μl). The resulting solution was analysed by HPLC (using a 2-μl sample volume). The rest of the volume was used for semipreparative HPLC purification under optimal content of ACN in the mobile phase. The purified probe was collected, and the solvent was evaporated under reduced pressure. The residue was dissolved in 120 μl of water. Then, 2 μl of this solution was analysed by HPLC to check the final purity. Chromatograms and mass spectra are presented in Supporting Material (Figures S3 and S4)

Thermal denaturation studies of acridines freely in solution

Two complementary 18 bases-long ODNs were used for screening tests of acridines in solution. Sense oligonu-

cleotide ($\mathbf{C_L}$) was labelled by 6-carboxyfluorescein (FAM), antisense oligonucleotide ($\mathbf{T_L}$) was labelled by BHQ1. The first stock solution (10 mM) was prepared by dissolution of a corresponding acridine in dimethyl sulfoxide (DMSO). The second stock solution (0.8 mM) was prepared by dilution of the first stock solution in water. Working solutions were prepared by dilution of the second stock solution to seven different concentrations of acridine (400, 100, 50, 25, 6.25, 0.64 and 0.08 μM). Working solutions of acridines (5 μl) were added to the PCR buffer (pH 8.3, 20 mM Tris–HCl, 20 mM KCl, 5 mM $(NH_4)_2SO_4$) with $\mathbf{C_L}$ (0.15 μM) and $\mathbf{T_L}$ (0.30 μM) in the wells (15 μl) to get final concentrations of tested compounds (one fourth of the above-mentioned working solutions). The mixture was heated at 95°C for 1 min, and the mixture was cooled to 40°C during 3 min. Then, the temperature was slowly raised by increments of 0.2°C in temperature until it reached 80°C. Fluorescence was measured 5 s after every 0.2°C increment. Final values of fluorescence were plotted against temperature to get melting curves. Melting curves were compared to the control without acridine. The comparison of the melting peaks gave ΔT_m. The tests were performed in triplicate and the data in Figure 3 and Table 1 represent mean ± standard deviation (SD).

Fluorescence-based thermal denaturation studies of the probes modified by FAM and acridine

ODN probes labelled with FAM and with/without acridine were tested on CFX96 Touch Real-Time PCR thermal cycler (Bio-Rad, Hercules, CA, USA). A 96-well plate was used for determination of melting temperature (with fluorescence channel for FAM, λ_{ex} = 450–490 nm, λ_{em} = 515–530 nm). PCR buffer with antisense ODN labelled with BHQ1 (15 μl, 0.53 μM) was transferred to the well plate. The working solution of the probes modified by FAM and acridine (5 μl, 1.2 μM) was added to the buffer in the wells to get final concentration of the modified probes (0.3 μM) and the antisense ODN (0.4 μM). The mixture was heated at 95°C for 1 min, and the mixture was cooled to 40°C during 3 min. Then, the temperature was slowly raised by increments of 0.2°C until it reached 80°C. Fluorescence was measured 5 s after every 0.2°C increment of the temperature was reached. Final values of fluorescence were plotted against temperature to get melting curves. All experiments were performed in triplicate.

Absorption-based thermal denaturation studies of the probes modified by FAM and acridine

Modified ODN probes were tested on Shimadzu UV-2600 spectrophotometer coupled with Shimadzu S-1700 temperature controller (Shimadzu, Kyoto, Japan). A 1400-μl absorption quartz cuvette was used for determination of melting temperature. PCR buffer with ODN labelled with BHQ-1 and probe modified by FAM and acridine (1000 μl, 1 μM of both ODN strands) was transferred to the cuvette. The mixture was heated at 95°C for 3 min and then allowed to cool slowly to room temperature for 10 minutes. The cuvette was placed in a holder heated to 40°C and absorption at 260 nm was measured after 90 s of stabilisation. Then, the temperature was raised by increments of 0.5°C until it reached 80°C. Absorbance was measured 90 s after every 0.5°C increment of the temperature was reached. Final values of absorbance were plotted against temperature to get melting curves. Prism 9 (GraphPad) software was used for melting peak analysis. All experiments were performed in triplicate.

Fluorescence-based thermal denaturation studies of the probes modified by acridine only

Acridine-modified ODN probes (**L_1_2***, **L_7_2*** and **S_1_2***) were tested on FLS1000 spectrofluorometer (Edinburgh Instruments, Edinburgh, UK). A 1400-μl fluorescence quartz cuvette was used for determination of melting temperature. PCR buffer with ODN labelled with BHQ-1 and the probe modified by acridine (1000 μl, 1 μM of both ODN strands) was transferred to the cuvette. The mixture was heated at 95°C for 3 min and then allowed to cool slowly to room temperature for 10 min. The cuvette was placed in a holder tempered to 20°C (for **S** probes) or 40°C (for **L** probes) and fluorescence at λ_{em} = 500 nm was measured after 90 seconds of stabilisation (λ_{ex} = 400 nm). Then, the temperature was slowly raised by increments of 0.5°C until it reached 60°C (for **S** probe) or 80°C (for **L** probes). Fluorescence was measured 90 seconds after every 0.5°C increment of the temperature was reached. Final values of fluorescence were plotted against temperature to get melting curves. Prism 9 (GraphPad) software was used for melting peak analysis. All experiments were performed in triplicate.

Study of interaction of acridine 2 with ssDNA and dsDNA

A 4-mM stock solution of acridine derivative **2** in water was prepared. 5 μl of this stock solution was added to 995 μl of reaction buffer (10 mM Tris–HCl (pH 7.5 at 25°C), 2.5 mM $MgCl_2$, 0.1 mM $CaCl_2$) to give 1000 μl of a 20 μM solution of **2** in cuvette. The 20-μM solution of **2** in reaction buffer was used for a UV–Vis monitored DNA binding study. Absorption spectrum at wavelength range 350–500 nm of the solution was measured after each small addition of ssDNA or dsDNA (stock solution concentration was 1 mM) until the final concentration of ssDNA or dsDNA was 40 and 20 μM, respectively. Sequences of ODNs are mentioned in 2. In case of fluorescence measurements (FLS1000 spectrofluorometer (Edinburgh Instruments)), the emission spectrum was monitored at wavelength range 390–700 nm after excitation at λ_{ex} = 380 nm.

Job's plot

Stock solution of acridine **2** (20 μM) and stock solutions of dsHFE, dsAT, dsGC and ssHFE (20 μM) in a reaction buffer (10 mM Tris–HCl (pH 7.5 at 25°C)) were prepared. A solution of acridine **2** and a corresponding solution of ds or ssDNA were mixed in various ratios to give 1 ml of the mixture each time. Simultaneously, the stock solution of acridine **2** was mixed with the reaction buffer (without ds or ss DNA) in the same ratios to give 1 ml of mixture. Absorption spectra of the solutions were measured at wavelength range 350–500 nm. Absorbance of the mixture of acridine

2 and ds or ssDNA at wavelength 417 nm was subtracted from absorbance of acridine **2** in the mixture with reaction buffer at the same wavelength. This change in absorbance was plotted against $c_{acr}/(c_{acr} + c_{DNA})$; where c_{acr} is the concentration of the acridine, and c_{DNA} is the concentration of ds or ssDNA.

Hybridisation study of the ODN with covalently tethered acridine 2

Solution of **L_7_2*** (10 μM) was prepared in reaction buffer and used for UV–Vis, and fluorescence monitoring of the hybridisation and spectral changes of the acridine interaction with ssDNA and dsDNA. Absorption spectra at wavelength range 350–500 nm, and fluorescence spectra at wavelength range 420–650 nm (λ_{ex} = 400 nm) of the solution were measured after each small addition and hybridisation of complementary $\mathbf{T_L}$ not labelled by BHQ-1 (stock solution concentration was 2 mM) until the final concentration of complementary strand reached 20 μM. The ODN was hybridised according to the following procedure: the mixture was heated at 95°C for 3 min and then allowed to cool slowly to room temperature for 10 min. The procedure was repeated after every addition of the $\mathbf{T_L}$.

Study of temperature-dependent changes of emission spectra of L_7_2*

Temperature maps of emission spectra (420–700 nm) were measured on FLS1000 spectrofluorometer (Edinburgh Instruments). A 1400-μl fluorescence quartz cuvette was used for measurements of temperature maps. $\mathbf{T_L}$ (1 μl of 1 mM stock solution) was added to the solution of **L_7_2*** (1 μM) in PCR buffer (1000 μl). The mixtures were heated at 95°C for 3 min and then allowed to cool slowly to room temperature for 10 min. The cuvette was placed in a holder cooled to 40°C, and emission spectra (420–700 nm) were measured after 90 s of stabilisation (λ_{ex} = 400 nm). Then, the temperature was raised by increments of 1.0°C until it reached 80°C. Emission spectra were measured 90 s after every 1.0°C increment of the temperature was reached.

Melting analysis of HFE gene template

Real-time PCR and melting analysis were performed using a CFX96T Cycler (Bio-Rad) (with fluorescence channel for FAM, λ_{ex} = 450–490 nm, λ_{em} = 515–530 nm) in a gb Basic PCR master mix with 2 mM concentration of Mg^{2+} in reaction. All components were mixed prior to PCR start (forward primer (0.1 μM), reverse primer (0.5 μM), quenching sequence with BHQ-1 (0.2 μM), fluorescent probe **L_7_2** (0.15 μM) and the template (1×10^5 copies)). The temperature profile of the PCR reaction was as follows: initial denaturation at 95°C for 3 min and 50 cycles of denaturation at 95°C for 10 s, followed by annealing and elongation at 60°C for 10 s and 72°C for 20 s. The melting analysis followed immediately: 95°C for 1 min; 35°C for 3 min, melting curve from 35 to 80°C with 0.5°C increment in 5 s. The probes and primers were based on a quantification assay for the HFE gene with the following sequences: forward primer: GGACCTTGGTCTTTCCTTGTTTG, reverse primer: CACATCTGGCTTGAAATTCTACTGG, fluorescent probe (**L_7_2**): TGATCATGAGAGTCGCCG, and the quenching sequence (labeled by a BHQ-1 quencher on 3-end): ATGGATGACCAGCTGTTCGTGTTC. For sequence of the templates (wild-type, C > G and A > T mutants), see Figure 7A. All experiments were performed in triplicate.

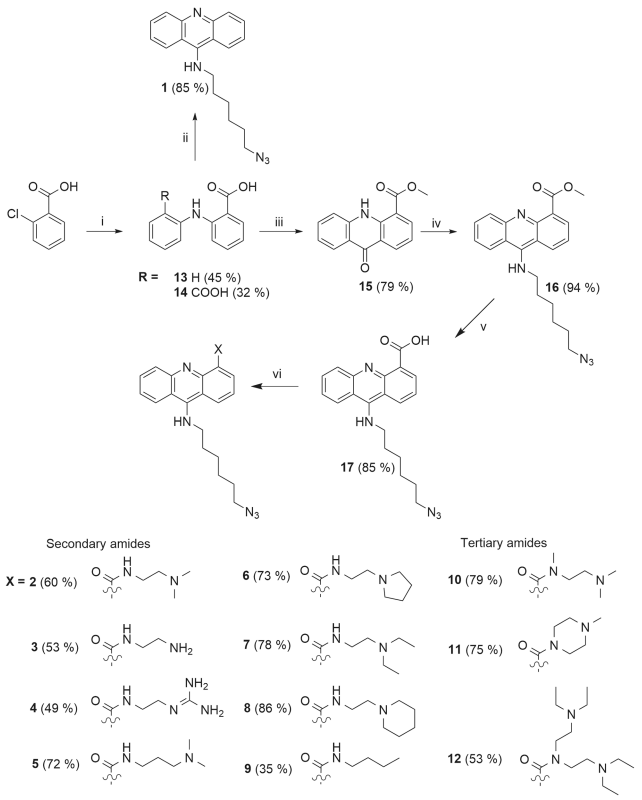

Scheme 1. Synthesis of acridine modifiers. Reaction conditions: i) Cu^0, K_2CO_3, isopentyl alcohol, aniline (for **13**) or anthranilic acid (for **14**), reflux overnight; ii) 1. **13**, $POCl_3$, reflux, 1 h; 2. phenol, 110°C, 15 min; 3. 6-azidohexyl-1-amine, 55°C, overnight; iii) 1. **14**, $POCl_3$, reflux, 1 h; MeOH, 50°C, overnight; iv) 1. $SOCl_2$, 80°C, 1 h; 2. phenol, 110°C, 15 min; 3. 6-azidohexyl-1-amine, 55°C, overnight; v) THF, excess of saturated solution of NaOH in MeOH:H_2O 5:1, 50°C, 1 h; vi) 1. $SOCl_2$, rt, 1 h; 2. Amine (1 equiv.), TEA (4 equiv.), DCM, 0°C, 30 min. Compounds **2**–**12**, except compound **9**, were converted to corresponding hydrochlorides.

RESULTS AND DISCUSSION

Design and synthesis of acridines

Structures of acridine-4-carboxamide derivatives in this study were inspired by compounds with high binding affinity to duplex DNA where high effect on the stabilisation of the DNA was expected (31). In our study, the side chain on the carboxamide was modified to contain various basic motifs to compare their effect on the thermal stability and melting temperature of short ODN probes. Twelve acridine derivatives (**1**–**12**, Scheme 1) with 6-azidohexylamine linker suitable for possible attachment of the acridine to ODN probe by click chemistry were therefore prepared. The linker should provide sufficient flexibility for interaction of acridine moiety with probe-target duplex (52).

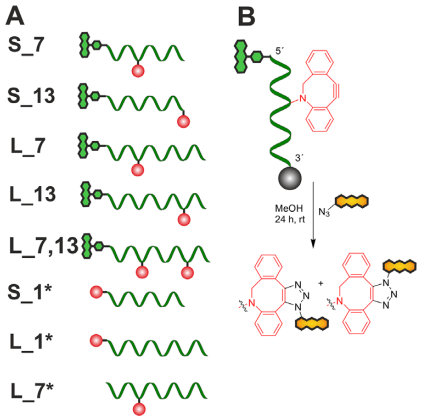

Scheme 2. (**A**) Schematic illustration of the modified probes. (**B**) Principle of 'click' modification of the probes on solid phase support. Dark-green dot–FAM, red dot–DBCO, grey dot–solid phase support, yellow stick–acridine modifier. **S** refers to 'short' and **L** to 'long' probe having 13 and 18 bases, respectively; numbers 1, 7 or 13 indicate the position of the acridine in the ODN probe.

Probe	Probe sequence
S_1*	5′-[DBCOdT]GA TCA TGA GAG T-3′-Phos
S_7	FAM-5′-TGA TCA [DBCOdT]GA GAG T-3′-Phos
S_13	FAM-5′-TGA TCA TGA GAG [DBCOdT]-3′-Phos
L_1*	5′-[DBCOdT]GA TCA TGA GAG TCG CCG-3′-Phos
L_7	FAM-5′-TGA TCA [DBCOdT]GA GAG TCG CCG-3′-Phos
L_7*	5′-TGA TCA [DBCOdT]GA GAG TCG CCG-3′-Phos
L_13	FAM-5′-TGA TCA TGA GAG [DBCOdT]CG CCG-3′-Phos
L_7,13	FAM-5′-TGA TCA [DBCOdT]GA GAG [DBCOdT]CG CCG-3′-Phos

Control	Control sequence
C_S	FAM-5′-TGA TCA TGA GAG T-3′-Phos
C_L	FAM-5′-TGA TCA TGA GAG TCG CCG-3′-Phos

Target code	Target sequence
T_S	5′-ACT CTC ATG ATC A-3′-BHQ1
T_L	5′-CGG CGA CTC TCA TGA TCA-3′-BHQ1
$T_{S(A)}$	5′-ACA CTC ATG ATC A-3′-BHQ1
$T_{S(C)}$	5′-ACT CTC ATC ATC A-3′-BHQ1
$T_{L(A)}$	5′-CGG CGA CAC TCA TGA TCA-3′-BHQ1
$T_{L(C)}$	5′-CGG CGA CTC TCA TCA TCA-3′-BHQ1

Chart 1. Sequences of the probes, the controls, and the targets used in the study. Probes contain DBCO-modified T-base used for 'click' modification. * Probes without FAM labelling. **S** – short (13 bases), **L** – long (18 bases) ODNs. Numbers 1, 7 and 13 indicate the position of the acridine in the ODN probe. Phos = phosphate.

Synthesis started by Ullmann condensation of 2-chlorobenzoic acids with aniline or anthranilic acid to obtain precursors **13** and **14**, respectively (Scheme 1). (53) These anthranilic acid derivatives were then cyclised to corresponding acridones (e.g. **15** from **14**) (33) that were subsequently converted to 9-chloroacridines and immediately *in situ* modified by 6-azidohexylamine to give acridine **1** and intermediate **16** used for further functionalisation. (31) The methyl ester **16** was hydrolysed to **17** and used as a starting material for synthesis of acridine derivatives **2**–**12** (Scheme 1). In the first attempts, the acid **17** was activated by (1*H*-benzotriazol-1-yloxy) (dimethylamino)-*N,N*-dimethylmethaniminium hexafluorophosphate (HBTU) and the corresponding amine was added to the reaction mixture. Unfortunately, the yields of the final compounds were low (maximum 33%), and in the case of tertiary amides **10**–**12**, the synthesis was not successful at all. The synthetic procedure was therefore modified by use of thionyl chloride for conversion of the free carboxylic acid in **17** to acyl chloride with subsequent addition to the solution of corresponding amine and triethylamine (TEA) as the base. The synthetic procedure using thionyl chloride resulted in increased yields of the final compounds compared to the HBTU procedure (see Supporting Material, Table S1) and enabled preparation of all intended derivatives. Compounds **2**–**12** (except compound **9**) bearing aliphatic amines were subsequently converted to corresponding hydrochlorides (for increased solubility in MeOH used for the click reaction) where besides the basic aliphatic amine in the side chain, also the secondary 9-amino group on acridine was protonated.

Preparation of ODN probes

ODN probes covalently modified by selected acridines were prepared by click chemistry (Scheme 2). Probes were designed as a part of HFE gene containing two sites of known single nucleotide polymorphisms (Chart 1) (54,55). Ultramild phosphoramidite monomers were used for synthesis of the probes in the RNA/DNA synthesizer due to the known instability of the carbon-nitrogen bond in the amino group in position 9 of the acridine modifiers in the presence of NH_4OH that is typically used during the final cleavage and deprotection of the probes (56). The cleavage and deprotection was therefore achieved by K_2CO_3. Fluorescein (FAM) was attached to the 5-end of ODN as a fluorescent label for the melting assays. Three probes were also designed without FAM labelling at 5-end (Chart 1) that is indicated in the designation by an asterisk. The dibenzoazacyclooctyne (DBCO) moiety was introduced into the probes as a DBCO-modified dT cyanoethyl phosphoramidite during the synthesis of the probes, which allowed using a copper-free click chemistry for modification of the probes by azide-containing acridines (Scheme 2). For this purpose, the selected acridines were dissolved in MeOH, mixed with the ODN probes on solid phase and simply shaken at rt for 24 h. Advantageously, this procedure allowed washing out the unreacted acridines from the solid phase and reusing them without any extensive purification. In this work, five selected probes (Chart 1, Scheme 2) differed in length (13 or 18 bases), position of modified T-base (position 1, 7 or 13), and the number of modified T-bases (one or two) to evaluate different factors that could potentially influence the degree of stabilisation of the duplex. Probes have a sense orientation corresponding to the wild-type sequence of the HFE gene (see Chart 1 and Figure 7A). In applications where an influence of mismatches was studied, the paired sequence (either a 3-BHQ1 oligonucleotides or minus strand of ds-DNA template in PCR) had an antisense orientation and thus a mismatch CC and AA was present in case of H63D C > G and S65C A > T mutation, respectively. Based on the screening in solution done with the whole series **1**–**12** (see below), three highly active acridines (**2**, **3**, and **4**), and one inactive acridine (**11**) were selected for modification of the probes. However, the labelling of probes by acridine **3** was not successful even after several repetitions of the reac-

Table 1. Increase of melting temperature of the duplex $\mathbf{C_L}$–$\mathbf{T_L}$ after addition of studied acridines (at $c = 6.25$ μM)

Compound	ΔT_m
1	2.07 ± 0.09
2	12.00 ± 0.19
3	9.93 ± 0.34
4	4.47 ± 0.43
5	3.60 ± 0.28
6	6.80 ± 0.0
7	5.13 ± 0.19
8	4.87 ± 0.33
9	0.27 ± 0.23
10	0.07 ± 0.09
11	0.07 ± 0
12	0.00 ± 0
17	0.13 ± 0

tion. There were no detectable peaks corresponding to the probe modified by acridine **3** on HPLC chromatogram and that is why only ODN probes modified by acridines **2**, **4** and **11** were finally tested.

After cleavage from solid phase, all probes were purified and analysed by HPLC using a Luna-PhenylHexyl column and triethylammonium acetate buffer in various ratios with acetonitrile as mobile phase. Separation conditions were optimised and used for semipreparative HPLC purification of the probes. The absorption spectra (Figure 2B) of the analysed probes had spectral features characteristic of the ODN chain (band at 260 nm), acridine modifier (450 nm) and FAM label (495 nm). Interestingly, two peaks of approximately the same intensity were always observed during the analysis of all probes containing one acridine (Figure 2A, S3). The peaks had the same absorption spectra (Figure 2B), and after isolation were characterized by the same m/z (Figure 2C). A plausible explanation is based on the presence of two constitutional isomers resulting from the click reaction of the acridines with unsymmetrical DBCO (Scheme 2) and is further supported by observation of three peaks (in 1:2:1 ratio) in case of probes **L_7,13_2** and **L_7,13_4** with two attached acridines.

Screening tests of acridine derivatives

A screen of the activity of synthesized acridines on the DNA duplex thermal stabilisation was first performed with the compounds **1**–**12** and **17** freely in solution (not attached to the ODN probe) to determine structure-activity relationships in the whole series and to select the suitable candidates for attaching to ODN. For this purpose, two complementary ODN probes $\mathbf{C_L}$ (with 5-FAM) and $\mathbf{T_L}$ (with 3-BHQ-1 quencher) containing the HFE gene sequence were used as a model melting system (see Chart 1). Their melting temperatures (T_m) were determined in the absence or presence of increasing concentration of the tested acridines.

The duplex melted typically at higher temperatures in the presence of the acridines. The increase ΔT_m was calculated as the difference between T_m with and without the acridines (Figure 3). For comparison purposes, the results were analysed as the ΔT_m at 6.25 μM concentration of acridine (see Table 1). The analysis of the data enabled drawing the following structure-activity relationships: (i) acridine derivatives containing tertiary carboxamide (**10**–**12**, Figure 3) did not increase melting temperature significantly even at the highest concentrations while those with secondary amides were effective. A hydrogen atom in the carboxamide group of acridine-4-carboxamides is most likely involved in a water-bridging hydrogen bond to the phosphate group in the DNA backbone (27). (ii) The absence of the basic moiety within the side chain of the secondary amides (**9**) or presence of carboxylic acid (**17**) led to complete loss of ability to increase melting temperature of the duplex as well. (iii) Compound **1** (no carboxamide moiety) also stabilised the ODN duplex slightly. However, the stabilisation was lower compared to all secondary amides **2**–**8**. Of note, the unsubstituted 9-aminoacridine linked to the peptide nucleic acid (PNA) has been utilized in thermal stabilisation of DNA–PNA duplexes already by other researchers (57). (iv) Distance of two carbons between carboxamide and the basic moiety seems to be optimal–its extension to 3 carbons in **5** led to a drop of the activity (compare with **2**). (v) The character of the basic moiety (most importantly its size) may also affect the results. Apparently, the smaller the basic group is, the higher the effect on stabilisation. For example, compounds **2** and **3** with dimethylamino and amino group, respectively, belonged to the most active while **7** and **8** with bigger diethylamino or piperidinyl had rather small effect.

DNA binding study

Based on the above-mentioned experiments, acridine **2** with the highest ΔT_m was selected for the interaction study with double-stranded (ds) and single-stranded (ss) DNAs. Three types of dsDNAs and ssDNAs (Chart 2) were used for titrations of acridine **2**, i.e. GC-rich, AT-rich and HFE sequence (mixed amount of GC and AT bases). After addition of dsDNA to the acridine **2** solution, bathochromic and hypochromic shifts in its absorption spectrum were observed (Figure 4A-C). Reduction of its fluorescence and change of emission spectra were observed as well (Figure 4E–G, S5) with more pronounced reduction observed for GC-rich and HFE duplex (Figure 4J). Such changes indicated an important π-π interaction of acridine heterocycle with nucleic bases. In line with our observations, Kim *et al.* described similar changes in absorption spectra of 9-aminoacridine bound to poly (dA).poly (dT) duplex. (58) Observed changes of emission spectra are also in concordance with changes in emission spectra of *N*-((*N*-(2-dimethylamino)ethyl)acridine-4-carboxamide)-α-alanine bound to calf thymus DNA described by Wu *et al.* (59) Interestingly, qualitative differences in the absorption and emission spectra were observed in case of **2** bound to either GC-rich or AT-rich duplex (Figure 4A, B, E, F), indicating slightly different interaction with these bases. Absorption and emission spectrum of **2** bound to HFE duplex was almost identical to the absorption and emission spectrum with the GC-rich duplex (Figure 4I, J) suggesting preference of **2** for GC interaction over the AT. In line with these observations, the quantitative data from absorbance (Figure 4D) also indicated a steeper binding isotherm in case of GC-rich and HFE duplexes, further confirming these conclusions. The quantitative data from fluorescence titrations indicated a steeper binding isotherm in the case of the GC-rich sequence al-

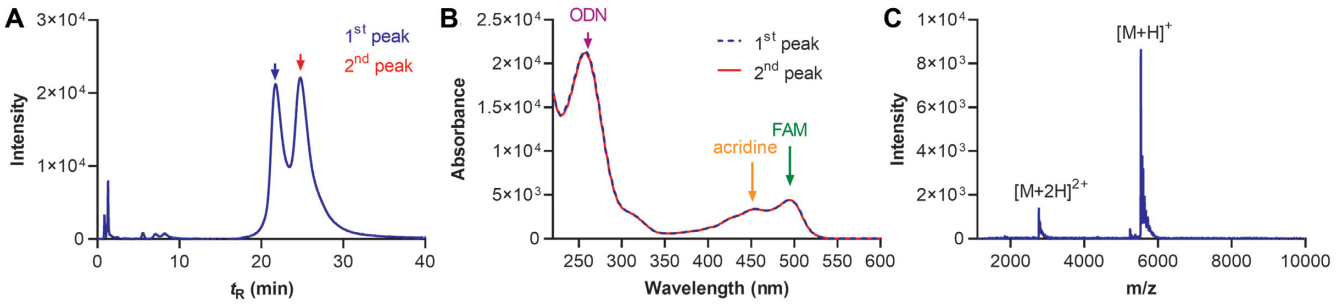

Figure 2. (**A**) Chromatogram of **S_7_2** (λ = 260 nm). (**B**) Absorption spectra of two peaks at chromatogram (A). (**C**) Mass spectrum of **S_7_2** probe.

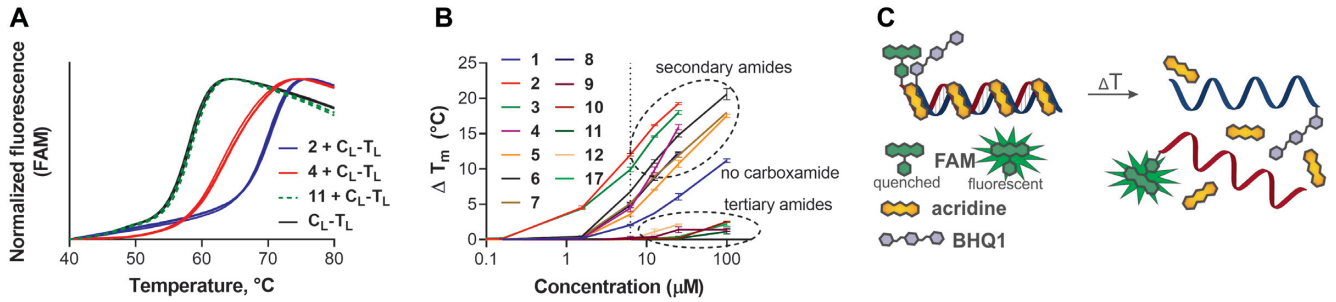

Figure 3. (**A**) Melting curves of the duplex $\mathbf{C_L}$–$\mathbf{T_L}$ alone (black) or with selected acridine derivatives, **2** (blue), **4** (red) and **11** (dashed green) at concentration 6.25 μM. (**B**) Screening test of acridine derivatives in the HFE melting system in solution expressed as dependence of the change of ΔT_m on the concentration of acridine. Vertical dotted line is drawn at $c = 6.25$ μM used for comparison purposes. The test was performed in triplicate. (**C**) Scheme of HFE melting system.

HFE duplex	5'-TGATCATGAGAGTCGCCG-3' ACTAGTACTCTCAGCGGC
GC-rich duplex	5'-TCCAGGGGTCCCGCCAGC-3' AGGTCCCCAGGGCGGTCG
AT-rich duplex	5'-TATATTTATAGTTCTTTA-3' ATATAAATATCAAGAAAT

Chart 2. ODNs duplexes used for study of interaction of acridine **2** with ODNs. Sense strands (used as ssDNAs in the study) are marked by a red panel.

though the difference between the binding isotherms of the GC-rich and AT-rich sequences was less pronounced compared to data obtained from absorbance titrations (Figure 4D, H). A plausible explanation was put forth by Finlay *et al.* (60) In their work, they suggested that the carboxamide side chain is expected to be exposed to the major groove, the fact that was confirmed later by crystallographic data. (61) As the major groove is deeper in the GC region, it allows tighter binding in the GC and results in preference of GC over AT due to interference with thymine methyl groups.

Interaction of **2** with the three types of ssDNA was also studied. Although the studied ssDNAs can also potentially form the double-stranded self-structures, they are too weak to be stable at the studied temperature, as confirmed by the absorption-based melting study of the concerned ssDNAs where no significant changes were observed, confirming that ssDNAs did not form any secondary structures at a significant level (Supplementary Figure S7). Changes in absorption and emission spectra of **2** titrated by ssDNA (Supplementary Figure S5) resembled those observed for dsDNA. Hypochromic and bathochromic shifts were observed during absorbance titrations by all types of ssDNA, again with slight differences between AT-rich and GC-rich sequences (Supplementary Figure S5). Absorption spectra were also slightly blue-shifted when compared to the dsDNAs (Supplementary Figure S5). However, the differences in binding isotherms between GC-rich, AT-rich and HFE sequences of ssDNA were almost not detected. In comparison with corresponding isotherms in interaction with dsDNA, they were substantially less steep, indicating weaker interaction (Figure 4D). In case of emission spectra, the differences in binding isotherms between GC-rich, AT-rich and HFE sequences of ssDNA (Supplementary Figure S5H) were more pronounced compared to binding isotherms of dsDNAs or compared to the binding isotherms of ssDNAs obtained from absorbance measurements (Supplementary Figure S5G). The emission and absorption spectrum of **2** bound to ssHFE was almost identical to the spectrum with ssGC (Supplementary Figure S5J, K). All these results indicated high preference of **2** for GC-rich strand also in ssDNA (Supplementary Figure S5L). Considering the mode of interaction, the acridines were suggested to interact with ssDNA by electrostatic forces or by dye-base stacking. (62) Based on the observed similarity of the results for ssDNA with dsDNA, the latter explanation is more probably since the dye-base stacking may lead to similar spectral response as in the case of intercalation into dsDNA.

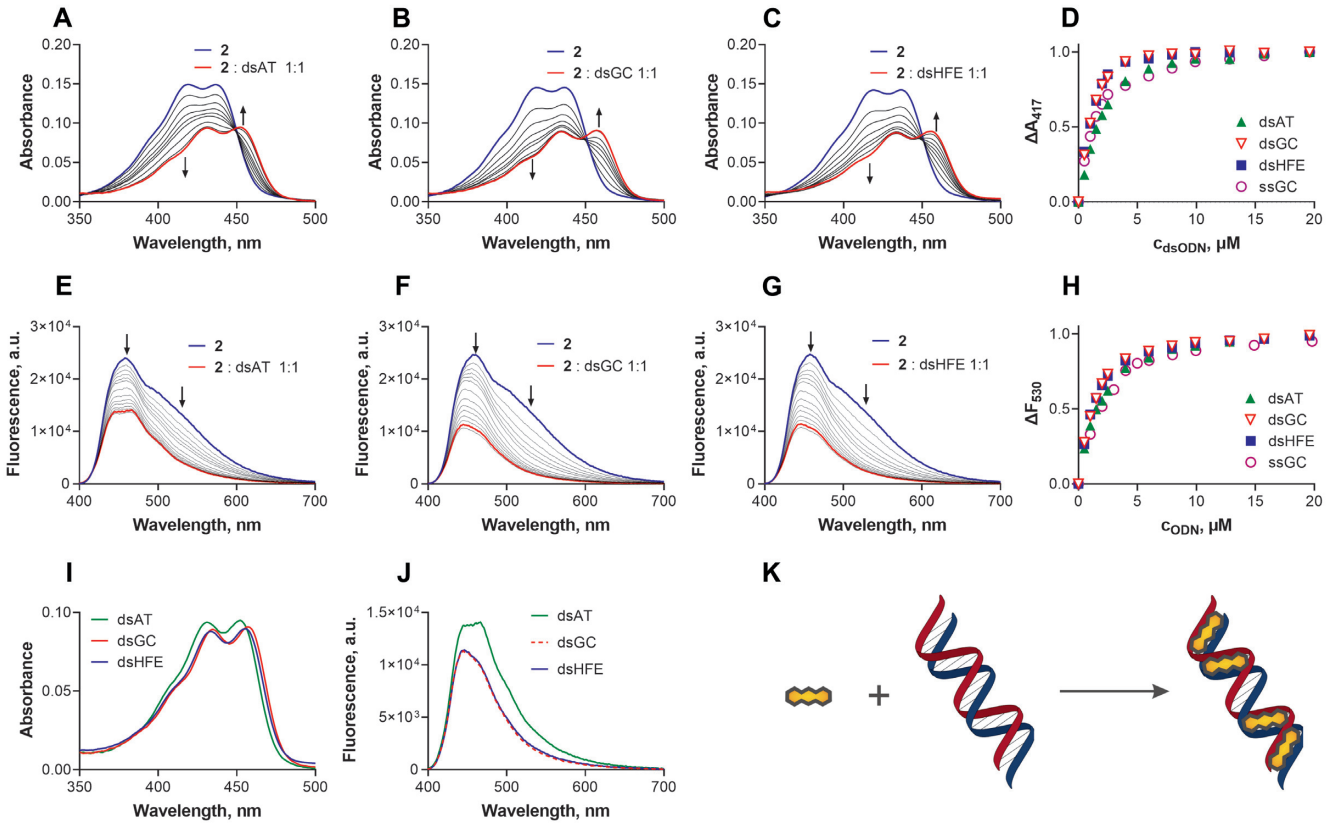

Figure 4. Changes in absorption (**A**–**C**) and emission (**E**–**G**) spectra (λ_{ex} = 380 nm) of acridine **2** (20 μM) during the titration by AT-rich (A, E), GC-rich (B, F), and HFE (C, G) duplexes in reaction buffer. (D, H) Changes in absorption at 417 nm (D) and emission at 530 nm (H) of acridine **2** during the titration by duplexes (AT-rich–green, GC-rich–red, HFE–blue), and ssGC-rich (purple). (**I, J**) Comparison of absorption (I) and emission (J) spectra of **2** (20 μM) complexed to AT-rich (green), GC-rich (red) and HFE (blue) duplexes (20 μM). (**K**) Schematic principle of the experiment.

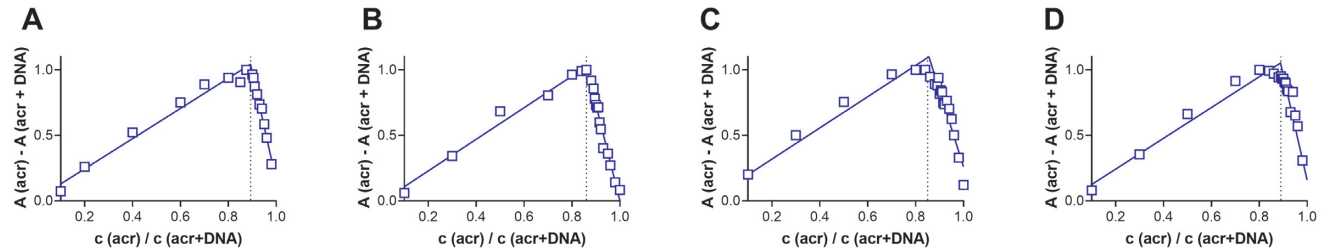

Figure 5. Job's plot of the interaction of **2** with (**A**) dsHFE, (**B**) ssHFE, (**C**) dsAT, (**D**) dsGC (monitored as absorption of acridine at 417 nm).

To examine the stoichiometry of binding of **2** to ssHFE and three types of dsDNAs, Job's plot was performed. From the constructed plots (Figure 5A-D), approximately nine molecules of **2** are obviously bound to one 18-bases long ssHFE or duplexes, indicating that acridine **2** is bound to DNA single strand or duplex *per* every second base pair.

Thermal denaturation studies of probes labelled by FAM and acridine

After tests in solution, the effect of acridines directly attached to the FAM-labelled probes on the thermal stabilisation was examined. The probes (Scheme 2, Chart 1) differed in length (13 bases (**S**), 18 bases (**L**)), type (acridine **2**, **4** or **11**) and position of the tethered acridine within the sequence (position 7 or 13). All probes labelled with FAM and acridine were tested in an HFE thermal denaturation system with complementary target ODNs ($\mathbf{T_S}$, $\mathbf{T_L}$ with 13 and 18 bases, respectively) and later also with complementary sequence with two different mismatches. Melting curves of all probes had sigmoidal shape comparable with the melting curve of unmodified control probes (Figure 6A). Acridine-modified probes exerted seemingly two transitions (e.g. Figure 6B, at approximately 53°C for **L_7_4**). Artefacts at the beginning of melting curves may be caused by local melting of potential interaction between FAM and acridine and were dependent on the position of the modification. In Figure 6B, when comparing the oligonucleotide curves, **L_7_4** has these artefacts more pronounced than **L_13_7**. **L_7_4**

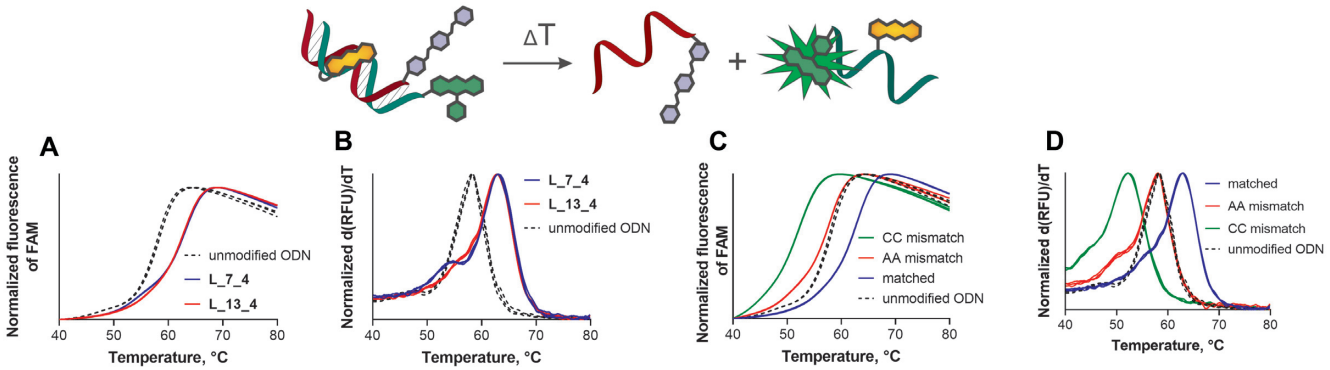

Figure 6. (**A**) Comparison of melting curves and corresponding melting peaks (**B**) of the **L_7_4** (blue), **L_13_4** (red) in duplex with $\mathbf{T_L}$ and control unmodified duplex $\mathbf{C_L}$–$\mathbf{T_L}$ without acridine moiety (black, dashed). (**C**) Comparison of melting curves and corresponding melting peaks (**D**) of **L_13_4** matched to the target $\mathbf{T_L}$ (blue), **L_13_4** hybridised to the A mismatched target $\mathbf{T_{L(A)}}$ (red), **L_13_4** hybridised to the C mismatched target $\mathbf{T_{L(C)}}$ (green), and control unmodified perfectly matched duplex $\mathbf{C_L}$–$\mathbf{T_L}$ without acridine moiety (black, dashed). All melting curves were measured at the channel for FAM (λ_{em} = 515–530 nm). All measurements were performed in triplicate.

carries the acridine modification bound closer to FAM at the 5 end than **L_13_4**, and it is likely that this closer position may manifest itself in more pronounced artefacts at the beginning of the melting curve. These artefacts, however, did not affect the determinations of the melting temperatures.

Melting temperature (T_m) of duplexes with all acridine-modified probes was increased compared to the melting temperature of duplexes with unmodified control ODNs ($T_{m\,(0)}$) (Table 2). Melting temperature of the long probes (**L**) increased typically between 4–5°C while the increase in short probes (**S**) was between 6–7°C with **S_13_2** being the best modification ($\Delta T_{m\,(0)} = 7.8 \pm 0.24$°C). This observation was expected, due to the greater absolute contribution of the modifier to the binding energy of short probes compared to longer probes. No unequivocal differences were observed between probes modified by acridine **2** and **4** (Table 2). The position (7 or 13) of the modifier within the sequence of both **S** and **L** probes also seem not to significantly affect $\Delta T_{m\,(0)}$ of the matched duplexes. As a negative control, **L_7_11** modified by inactive acridine derivative **11**, was also prepared and studied. Only very low increase ($\Delta T_{m\,(0)} =$ 1.7°C) of melting temperature was observed for this probe.

Interestingly, double labelling of the **L** probes by acridines (**L_7,13_2** and **L_7,13_4**) also led to the shift of the fluorescence-based melting curves toward the higher temperatures (see melting curves, Supplementary Figure S6A), but the shape of the curves was altered and did not allow unequivocal analysis of the melting peaks after derivatization (Supplementary Figure S6B) for which we have no clear explanation right now. As an alternative, we also performed absorption-based analysis of the melting temperatures. As the absorption is less sensitive, the experiments had to be performed at higher concentrations (1 μM for absorption while 0.3 μM for fluorescence measurements) that slightly changed the basal $T_{m\,(0)}$ for approximately 1.6°C. First, we compared the fluorescence and absorption-based data for two probes modified by one acridine only (**L_13_2** and **L_7_4**) and found the ΔT_m values to be comparable with fluorescence-based data that confirmed that both methods will give the same results (Supplementary Table S2). Subsequently, the double-labelled probes were tested. Contrary to the observation in fluorescence experiments, the shape of absorption-based melting curves was not altered and allowed unequivocal analysis of the melting peak after derivatization (Supplementary Figure S6C, D). Melting temperatures of duplexes of double labelled probes **L_7,13_2** and **L_7,13_4** with $\mathbf{T_L}$ were increased by $\Delta T_{m\,(0)}$ = 6.6°C and 7.0°C, respectively (Supplementary Table S2), i.e. even higher than for single acridine modified probes, indicating increased stabilising effect of additional acridine. However, despite this beneficial effect, the further practical use of this modification is limited by impossibility of fluorescence analysis of T_m and that is why these probes were not investigated further.

Based on these encouraging results, the effect of the modifier on mismatch discrimination ability was evaluated. Two mismatched target sequences of the HFE gene were selected, H63D C > G (rs1799945, c.187) and S65C A > T (rs1800730, c.193). Both mutations are associated with hereditary hemochromatosis type 1. (54,55) The melting temperatures of these mismatched ODNs ($\mathbf{T_{S(A)}}$, $\mathbf{T_{S(C)}}$, $\mathbf{T_{L(A)}}$, $\mathbf{T_{L(C)}}$, Chart 1) with acridine-modified probes were determined ($T_{m\,(A)}$, $T_{m\,(C)}$) and compared to the T_m of matched ODNs. In all cases, the mismatched duplexes melted at much lower temperature. In case of AA mismatch, the $\Delta T_{m\,(A)}$ values reached values approximately 8–9°C and 4–5°C for short and long probes, respectively. No obvious differences were observed between the probes, considering the position or structure of the acridine. In the case of CC mismatch, the differences in temperatures were more significant (up to $\Delta T_{m\,(C)} = 24.3$°C, Table 2) and clearly dependent on the position but not on the structure of acridine (results were almost the same for both **2** or **4**). When the acridine was placed in the position 13, it always stabilised the mismatched duplex less, leading to lower $T_{m\,(c)}$ and consequently higher $\Delta T_{m\,(C)}$ which enables better discrimination of the modification. In the case of CC mismatch, similarly to AA mismatch, the longer probes led to higher $T_{m\,(C)}$ and consequently also to less pronounced $\Delta T_{m\,(C)}$ that were more than half of the short probes. The presented data therefore revealed the excellent ability of the probes with acridine to discriminate between matched and

Table 2. Melting temperatures of modified probes.[a,b]

ODN code	$T_{m\,(0)}$ (°C)	T_m (°C)	$T_{m\,(A)}$ (°C)	$T_{m\,(C)}$ (°C)	$\Delta T_{m\,(0)}$ (°C)	$\Delta T_{m\,(A)}$ (°C)	$\Delta T_{m\,(C)}$ (°C)
S_7_2	38.3	44.0	35.5	25.3	5.7	8.5	18.7
S_13_2	38.3	46.2	38.2	21.7	7.8	8.0	24.5
S_7_4	38.3	45.7	37.3	28.0	7.3	8.3	17.7
S_13_4	38.3	45.2	36.2	21.2	6.8	9.0	24.0
L_7_2	58.3	62.0	57.6	53.2	3.7	4.4	8.8
L_13_2	58.3	62.3	57.9	51.2	3.9	4.4	11.1
L_7,13_2[c]	58.3	-	-	-	-	-	-
L_7_4	58.3	63.2	58.2	54.0	4.9	5.0	9.2
L_13_4	58.3	62.9	58.2	52.1	4.6	4.7	10.9
L_7,13_4[c]	58.3	-	-	-	-	-	-

[a]$T_{m\,(0)}$, melting temperatures of unmodified duplexes (i.e. $\mathbf{C_S}$-$\mathbf{T_S}$ or $\mathbf{C_L}$-$\mathbf{T_L}$); T_m, melting temperatures of duplexes of modified probes with fully complementary target (i.e. with $\mathbf{T_S}$ or $\mathbf{T_L}$); $T_{m\,(A)}$, melting temperatures of duplexes of modified probes with target sequence with A mismatch (i.e. with $\mathbf{T_{S(A)}}$ or $\mathbf{T_{L(A)}}$); $T_{m\,(C)}$, melting temperatures of duplexes of modified probes with target sequence with C mismatch (i.e. with $\mathbf{T_{S(C)}}$ or $\mathbf{T_{L(C)}}$); $\Delta T_{m\,(0)} = T_m - T_{m\,(0)}$, $\Delta T_{m\,(A)} = T_m - T_{m\,(A)}$, $\Delta T_{m\,(C)} = T_m - T_{m\,(C)}$. [b]Determined by fluorescence measurements in PCR thermal cycler. [c]The melting peak in fluorescence measurements could not be properly analysed for the modified probes. $\Delta T_{m\,(0)} = 6.6$°C and 7.0°C for **L_7,13_2** and **L_7,13_4**, respectively, were determined by absorption-based measurements.

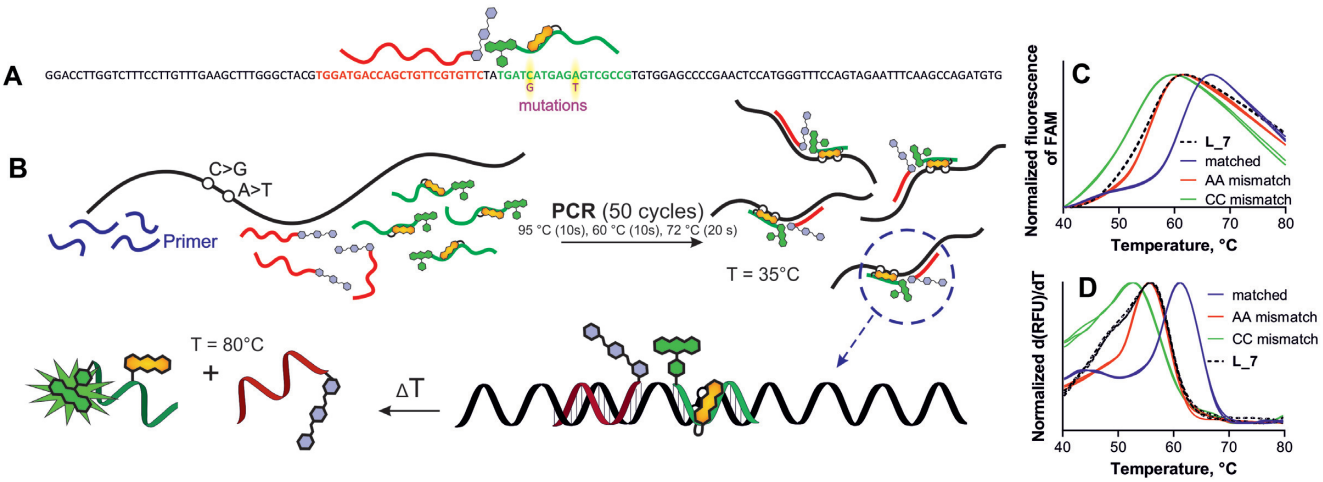

Figure 7. Determination of the potential mutations in the HFE gene in models of real samples. (**A**) Template containing HFE gene sequence. (**B**) Principle of the determination. (**C**) Melting curves and melt peaks (**D**) of the wild type of HFE (matched, blue) and its S65C A > T (red), and H63D C > G (green), determined with probe **L_7_2.** The control experiment with probe **L_7** (no acridine conjugation) and wild type HFE perfectly matched is shown by the black dashed line.

mismatched sequences in the HFE system. We also considered the fact that the acridine stabiliser may interact directly with the mismatch position, but it seems to be unlikely. High preference was observed for GC pair that is always near the T base modified by acridine and therefore it is expected that the acridine will intercalate primarily in the closest GC pair (the length of the linker is sufficient) where it has the highest preference. The mutations are also always in close proximity (2 bp) but it is expected that the preference for C–C or A–A bases will be lower.

The system was subsequently used in determination of the potential mutations in the HFE gene in models of real samples using adjacent probes (Figure 7B). Plasmids (linearized prior to use in PCR) with the cloned wild type or the mutated variant of HFE target sequence were used as templates for PCR. The fluorescent probe **L_7_2.** recognized the wild-type form and both potential A > T or C > G mutation. The template (1×10^5 copies) was subjected to PCR to multiply the template and then melting analysis was performed together with the sequence bearing BHQ-1 quencher that hybridised adjacent to the reporter probe. In line with the above experiments, good discrimination of both mutations was observed (Figure 7C, D).

Absorption and fluorescence study of intercalation of acridine 2 attached to the ODN

L_7_2* probe (without FAM to eliminate interference from its absorption and emission spectrum) was prepared to evaluate the intercalation properties of acridine **2** covalently attached to the probe, and its properties in the duplex. The fluorescence of acridine allowed monitoring of its fate using the emission spectra ($\lambda_{em} = 520$ nm, $\Phi_F = 0.49$ for **2** (in MeOH)). The solution of **L_7_2*** probe was titrated by $\mathbf{T_L}$ (without BHQ-1), and absorption and emission spectra were measured after every addition and hybridisation. In the beginning (without any $\mathbf{T_L}$), the spectrum of **L_7_2*** resembled the spectrum of acridine **2** after its interaction with ssODN HFE sense (Figure 8B, blue lines), indicating that the acridine in this probe interacts with the nucleic bases

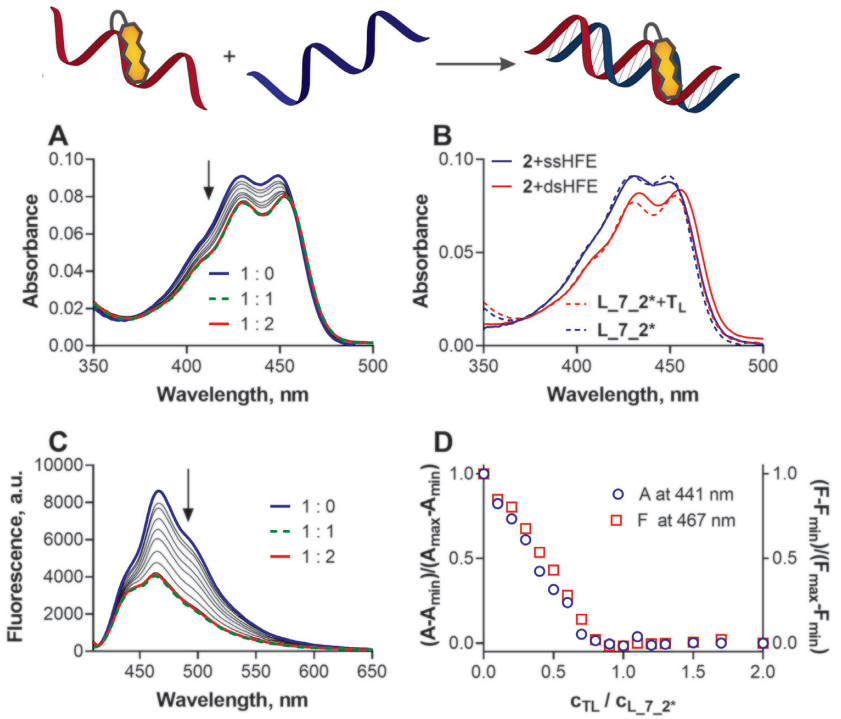

Figure 8. (**A**, **C**) Changes of absorption (**A**) and emission (**C**) spectra of **L_7_2*** probe titrated by $\mathbf{T_L}$; (**B**) Comparison of absorption spectra of **2** bound to ssHFE (blue) or dsHFE (red) freely in solution (full lines). Dashed lines are absorption spectra of **L_7_2*** with (red) or without (blue) complementary $\mathbf{T_L}$; (**D**) normalised changes in absorbance (blue) and fluorescence (red), of **L_7_2*** during titration with $\mathbf{T_L}$ (data from boxes A and C). Concentration of **L_7_2*** was 10 μM. $T = 23°C$.

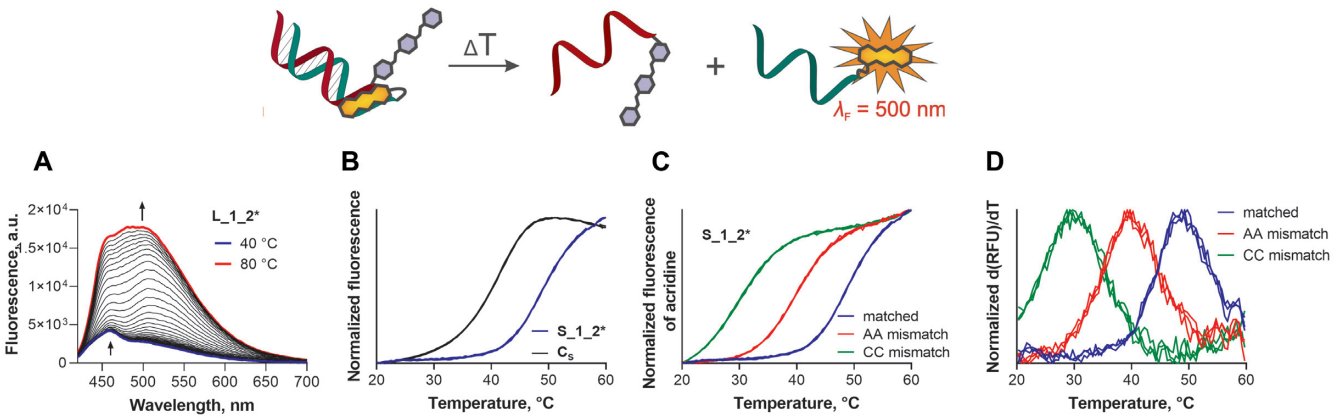

Figure 9. (**A**) Temperature dependent emission ($\lambda_{ex} = 400$ nm) changes of **L_1_2*** probe matched duplex with $\mathbf{T_L}$. (**B**) Comparison of melting curves of the **S_1_2*** (blue) and $\mathbf{C_S}$ (black) in duplex with $\mathbf{T_S}$. (**C**) Comparison of melting curves and melting peaks (**D**) of the **S_1_2*** matched to the target $\mathbf{T_S}$ (blue), **S_1_2*** hybridised to the A mismatched target $\mathbf{T_{S(A)}}$ (red), and **S_1_2*** hybridised to the C mismatched target $\mathbf{T_{S(C)}}$ (green).

already in the single strand before formation of a duplex. After stepwise addition of $\mathbf{T_L}$, minor changes in absorption spectra (bathochromic and hypochromic shift) were observed suggesting interaction of acridine with a newly formed duplex (Figure 8A), supported by the spectrum at full binding resembling the shape of the absorption spectra of acridine **2** bound to the dsODN HFE duplex (Figure 8A, B). The measurements of the fluorescence spectra showed a reduction in fluorescence intensity by 53% (the shape remained the same) after hybridisation with $\mathbf{T_L}$ (Figure 8C). In both absorption and fluorescence measurements, the changes progressed up to expected 1:1 ratio **L_7_2***: $\mathbf{T_L}$ with no further changes (Figure 8D). We can assume that these changes are due to the transition from intercalation in the ssODN to intercalation in dsODN with increased quenching of acridine by nucleic bases in duplex.

Due to inherent fluorescence of the acridine core, it could potentially be used as a fluorophore itself. This possibility was explored with three probes labelled by acridine **2** only (without FAM labelling)–**L_1_2***, **L_7_2*** and **S_1_2***. Ad-

Table 3. Melting temperatures of probes modified by acridine only obtained from fluorescence measurements[a]

ODN code	$T_{m\,(0)}$ (°C)	T_m (°C)	$T_{m\,(A)}$ (°C)	$T_{m\,(C)}$ (°C)	$\Delta T_{m\,(0)}$ (°C)	$\Delta T_{m\,(A)}$ (°C)	$\Delta T_{m\,(C)}$ (°C)
S_1_2*	41.3	49.0	39.3	29.5	7.7	9.7	19.5
L_1_2*	61.0	67.2	61.8	58.7	6.2	5.4	8.5
L_7_2*	61.0	65.6	58.7	58.1	4.6	6.9	7.5

[a] $T_{m\,(0)}$, melting temperatures of unmodified duplexes (i.e. $\mathbf{C_S}$–$\mathbf{T_S}$ or $\mathbf{C_L}$–$\mathbf{T_L}$); T_m, melting temperatures of duplexes of modified probes with fully complementary target (i.e. with $\mathbf{T_S}$ or $\mathbf{T_L}$); $T_{m\,(A)}$, melting temperatures of duplexes of modified probes with target sequence with AA mismatch (i.e. with $\mathbf{T_{S(A)}}$ or $\mathbf{T_{L(A)}}$); $T_{m\,(C)}$, melting temperatures of duplexes of modified probes with target sequence with CC mismatch (i.e. with $\mathbf{T_{S(C)}}$ or $\mathbf{T_{L(C)}}$); $\Delta T_{m\,(0)} = T_m - T_{m\,(0)}$, $\Delta T_{m\,(A)} = T_m - T_{m\,(A)}$, $\Delta T_{m\,(C)} = T_m - T_{m\,(C)}$.

ditional position 1 (i.e. 5-end) of modification by acridine was chosen since in the original design this position was dedicated to the fluorophore. Duplex of the probes with corresponding antisense strand $\mathbf{T_L}$ or $\mathbf{T_S}$ at 40°C was only weakly fluorescent both due to quenching of the intercalated acridine by nucleic bases (see Figure 9C) and by BHQ-1 quencher. Upon increase of the temperature, the fluorescence increased due to melting of the duplex and separation of the acridine from the quencher (Figure 9A, example for **L_1_2***). Melting curves plotted as a change of acridine fluorescence (λ_{ex} = 400 nm) at λ_{em} = 500 nm (the biggest change in the emission), had a sigmoidal shape comparable with unmodified control $\mathbf{C_L}$ (Figure 9B) but were shifted to higher temperatures due to stabilisation of the duplex with $\Delta T_{m\,(0)}$ = 7.9°C for short **S_1_2*** probe and 6.1°C and 4.3°C for **L_1_2*** and **L_7_2*** probes, respectively (Table 3). The probes were tested in a modified HFE thermal denaturation system with complementary target ODNs ($\mathbf{T_S}$, $\mathbf{T_L}$, Figure 9B) and also with complementary sequence with two different mismatches (Figure 9C, D). Also in this case, good discrimination of the mutations in HFE gene was observed (for ΔT_m see Table 3) in particular with the short **S_1_2*** probe (Figure 9C, D). Based on these results, the acridine can fulfil both functions in the probes–to stabilise the duplex and to serve as reporter dye due to its fluorescence.

Conclusions

In this work, a series of acridine derivatives was prepared and screened as the thermal stabilisers of the DNA duplexes. The structure–activity relationships revealed the strong importance of the presence of the secondary amide in position 4 and two-carbon linker to the basic moiety that should not be preferentially bulky. Selected acridines, once attached to the ODN probes labelled with FAM, were able to increase the melting temperature of the duplexes. They were also found suitable for discrimination of the mismatches where the high thermal stabilisation of the duplex was found only for matched sequences. Observations of the shape of absorption and emission spectra of the acridines suggested their intercalation interaction. Additionally, inherent fluorescence of acridine enabled its use as a fluorophore itself (without any other reported dye) and stabiliser at the same time therefore eliminating the necessity of the additional fluorophore (e.g. FAM). In conclusion, the selected acridines may be used as suitable thermal stabilisers and fluorophores of the DNA duplexes in particularly for short probes that may recognize single point mutations.

DATA AVAILABILITY

The original data from the article are available on Zenodo.org under doi: 10.5281/zenodo.6994174.

SUPPLEMENTARY DATA

Supplementary Data are available at NAR Online.

ACKNOWLEDGEMENTS

The authors wish to thank to Lucie Novakova for HR MS and Jiri Kunes for NMR measurements.

FUNDING

Charles University [SVV 260 547, GAUK 994218, PRIMUS/20/SCI/013]; European Regional Development Fund [CZ.02.1.01/0.0/0.0/16_019/0000841]. Funding for open access charge: Charles University [PRIMUS/20/SCI/013].

Conflict of interest statement. None declared.

REFERENCES

1. Kodama,S., Asano,S., Moriguchi,T., Sawai,H. and Shinozuka,K. (2006) Novel fluorescent oligoDNA probe bearing a multi-conjugated nucleoside with a fluorophore and a non-fluorescent intercalator as a quencher. *Bioorg. Med. Chem. Lett.*, **16**, 2685–2688.
2. Yamane,A. (2002) MagiProbe: a novel fluorescence quenching-based oligonucleotide probe carrying a fluorophore and an intercalator. *Nucleic Acids Res.,***30**, e97.
3. Kutyavin,I.V., Afonina,I.A., Mills,A., Gorn,V.V., Lukhtanov,E.A., Belousov,E.S., Singer,M.J., Walburger,D.K., Lokhov,S.G. and Gall,A.A. (2000) 3′-minor groove binder-DNA probes increase sequence specificity at PCR extension temperatures. *Nucleic Acids Res.,***28**, 655–661.
4. Chen,K., Kong,M., Liu,J., Jiao,J., Zeng,Z., Shi,L., Bu,X., Yan,Y., Chen,Y. and Gao,R. (2021) Rapid differential detection of subtype H1 and H3 swine influenza viruses using a taqman-MGB-based duplex one-step real-time RT-PCR assay. *Arch. Virol.*, **166**, 2217–2224.
5. Danielsen,M.B., Christensen,N.J., Jørgensen,P.T., Jensen,K.J., Wengel,J. and Lou,C. (2021) Polyamine-Functionalized 2′-Amino-LNA in oligonucleotides: facile synthesis of new monomers and high-affinity binding towards ssDNA and dsDNA. *Chem. Eur. J.*, **27**, 1416–1422.
6. Menzi,M., Wild,B., Pradère,U., Malinowska,A.L., Brunschweiger,A., Lightfoot,H.L. and Hall,J. (2017) Towards improved oligonucleotide therapeutics through faster target binding kinetics. *Chem. Eur. J.*, **23**, 14221–14230.
7. Qiu,J., Wilson,A., El-Sagheer,A.H. and Brown,T. (2016) Combination probes with intercalating anchors and proximal fluorophores for DNA and RNA detection. *Nucleic Acids Res.,***44**, e138.

8. Walsh,S., El-Sagheer,A.H. and Brown,T. (2018) Fluorogenic thiazole orange TOTFO probes stabilise parallel DNA triplexes at pH 7 and above. *Chem. Sci.*, **9**, 7681–7687.
9. Saady,A., Wojtyniak,M., Varon,E., Bo̎ttner,V., Kinor,N., Shav-Tal,Y., Ducho,C. and Fischer,B. (2020) Specific, sensitive, and quantitative detection of HER-2 mRNA breast cancer marker by fluorescent light-up hybridisation probes. *Bioconjugate Chem.,***31**, 1188–1198.
10. Emehiser,R.G. and Hrdlicka,P.J. (2020) Chimeric γPNA–Invader probes: using intercalator-functionalized oligonucleotides to enhance the DNA-targeting properties of γPNA. *Org. Biomol. Chem.*, **18**, 1359–1368.
11. Asseline,U., Toulme,F., Thuong,N.T., Delarue,M., Montenay-Garestier,T. and Hélène,C. (1984) Oligodeoxynucleotides covalently linked to intercalating dyes as base sequence-specific ligands. Influence of dye attachment site. *EMBO J.,***3**, 795–800.
12. Ranasinghe,R.T., Brown,L.J. and Brown,T. (2001) Linear fluorescent oligonucleotide probes with an acridine quencher generate a signal upon hybridisation. *Chem. Commun.*, **2001**, 1480–1481.
13. Ji,H., Johnson,N.P., von Hippel,P.H. and Marcus,A.H. (2019) Local DNA base conformations and ligand intercalation in DNA constructs containing optical probes. *Biophys. J.*, **117**, 1101–1115.
14. Orson,F.M., Kinsey,B.M. and McShan,W.M. (1994) Linkage structures strongly influence the binding cooperativity of DNA intercalators conjugated to triplex forming oligonucleotides. *Nucleic Acids Res.,***22**, 479–484.
15. Klysik,J., Kinsey,B.M., Hua,P., Glass,G.A. and Orson,F.M. (1997) A 15-base acridine-conjugated oligodeoxynucleotide forms triplex DNA with its IL-2Rα promoter target with greatly improved avidity. *Bioconjugate Chem.,***8**, 318–326.
16. Shinozuka,K., Seto,Y. and Sawai,H. (1994) A novel multifunctionally labelled DNA probe bearing an intercalator and a fluorophore. *J. Chem. Soc., Chem. Commun.*, **1994**, 1377–1378.
17. François,J.-C. and Hélène,C. (1999) Recognition of hairpin-containing single-stranded DNA by oligonucleotides containing internal acridine derivatives. *Bioconjugate Chem.,***10**, 439–446.
18. Fukui,K., Iwane,K., Shimidzu,T. and Tanaka,K. (1996) Oligonucleotides covalently linked to an acridine at artificial abasic site: influence of linker length and the base-sequence. *Tetrahedron Lett.,***37**, 4983–4986.
19. Fukui,K. and Tanaka,K. (1996) The acridine ring selectively intercalated into a DNA helix at various types of abasic sites: double strand formation and photophysical properties. *Nucleic Acids Res.,***24**, 3962–3967.
20. Asseline,U., Bonfils,E., Dupret,D. and Thuong,N.T. (1996) Synthesis and binding properties of oligonucleotides covalently linked to an acridine derivative: new study of the influence of the dye attachment site. *Bioconjugate Chem.*, **7**, 369–379.
21. Fukui,K., Morimoto,M., Segawa,H., Tanaka,K. and Shimidzu,T. (1996) Synthesis and properties of an oligonucleotide modified with an acridine derivative at the artificial abasic site. *Bioconjugate Chem.*, **7**, 349–355.
22. Balbi,A., Sottofattori,E., Grandi,T., Mazzei,M., Abramova,T.V., Lokhov,S.G. and Lebedev,A.V. (1994) Synthesis and complementary complex formation properties of oligonucleotides covalently linked to new stabilising agents. *Tetrahedron*, **50**, 4009–4018.
23. Balbi,A., Sottofattori,E., Grandi,T., Mazzei,M., Pyshnyi,D.S., Lokhov,S.G. and Lebedev,A.V. (1997) Synthesis and hybridisation properties of the conjugates of oligonucleotides and stabilisation agents—II. *Bioorg. Med. Chem.*, **5**, 1903–1910.
24. Sakore,T.D., Jain,S.C., Tsai,C.C. and Sobell,H.M. (1977) Mutagen-nucleic acid intercalative binding: structure of a 9-aminoacridine: 5-iodocytidylyl (3'-5')guanosine crystalline complex. *Proc. Natl. Acad. Sci. U.S.A.*, **74**, 188.
25. Adams,A., Guss,J.M., Collyer,C.A., Denny,W.A. and Wakelin,L.P.G. (1999) Crystal structure of the topoisomerase II poison 9-Amino-[N-(2-dimethylamino)ethyl]acridine-4-carboxamide bound to the DNA hexanucleotide d (CGTACG)2. *Biochemistry*, **38**, 9221–9233.
26. Rehn,C. and Pindur,U. (1996) Molecular modeling of intercalation complexes of antitumor active 9-aminoacridine and a [d, e]-anellated isoquinoline derivative with base paired deoxytetranucleotides. *Monatsh. Chem./Chem. Monthly*, **127**, 645–658.
27. Adams,A., Guss,J.M., Denny,W.A. and Wakelin,L.P. (2002) Crystal structure of 9-amino-N-[2- (4-morpholinyl) ethyl]-4-acridinecarboxamide bound to d (CGTACG) 2: implications for structure–activity relationships of acridinecarboxamide topoisomerase poisons. *Nucleic Acids Res.,***30**, 719–725.
28. Baguley,B.C., Denny,W.A., Atwell,G.J. and Cain,B.F. (1981) Potential antitumor agents. 34. Quantitative relationships between DNA binding and molecular structure for 9-anilinoacridines substituted in the anilino ring. *J. Med. Chem.*, **24**, 170–177.
29. Atwell,G.J., Cain,B.F., Baguley,B.C., Finlay,G.J. and Denny,W.A. (1984) Potential antitumor agents. Part 43. Synthesis and biological activity of dibasic 9-aminoacridine-4-carboxamides, a new class of antitumor agent. *J. Med. Chem.*, **27**, 1481–1485.
30. Wakelin,L.P., Atwell,G.J., Rewcastle,G.W. and Denny,W.A. (1987) Relationships between DNA-binding kinetics and biological activity for the 9-aminoacridine-4-carboxamide class of antitumor agents. *J. Med. Chem.*, **30**, 855–861.
31. Howell,L.A., Gulam,R., Mueller,A., O'Connell,M.A. and Searcey,M. (2010) Design and synthesis of threading intercalators to target DNA. *Bioorg. Med. Chem. Lett.*, **20**, 6956–6959.
32. Silva,M.d.M., Macedo,T.S., Teixeira,H.M.P., Moreira,D.R.M., Soares,M.B., Pereira,A.L.d.C., Serafim,V.d.L., Mendonça-Júnior,F.J., Maria do Carmo,A. and de Moura,R.O. (2018) Correlation between DNA/HSA-interactions and antimalarial activity of acridine derivatives: proposing a possible mechanism of action. *J. Photochem. Photobiol. B*, **189**, 165–175.
33. Goodell,J.R., Madhok,A.A., Hiasa,H. and Ferguson,D.M. (2006) Synthesis and evaluation of acridine- and acridone-based anti-herpes agents with topoisomerase activity. *Bioorg. Med. Chem.*, **14**, 5467–5480.
34. Rewcastle,G.W., Atwell,G.J., Chambers,D., Baguley,B.C. and Denny,W.A. (1986) Potential antitumor agents. 46. Structure-activity relationships for acridine monosubstituted derivatives of the antitumor agent N-[2- (dimethylamino) ethyl]-9-aminoacridine-4-carboxamide. *J. Med. Chem.*, **29**, 472–477.
35. Todd,A.K., Adams,A., Thorpe,J.H., Denny,W.A., Wakelin,L.P. and Cardin,C.J. (1999) Major groove binding and 'DNA-Induced'Fit in the intercalation of a derivative of the mixed topoisomerase I/II poison N- (2- (Dimethylamino) ethyl) acridine-4-carboxamide (DACA) into DNA: X-ray. *J. Med. Chem.*, **42**, 536–540.
36. Gouveia,R.G., Ribeiro,A.G., Segundo,M.Â.S.P., de Oliveira,J.F., de Lima,M.d.C.A., de Lima Souza,T.R.C., de Almeida,S.M.V. and de Moura,R.O. (2018) Synthesis, DNA and protein interactions and human topoisomerase inhibition of novel spiroacridine derivatives. *Bioorg. Med. Chem.*, **26**, 5911–5921.
37. Krokidis,M.G., Molphy,Z., Efthimiadou,E.K., Kokoli,M., Argyri,S.-M., Dousi,I., Masi,A., Papadopoulos,K., Kellett,A. and Chatgilialoglu,C. (2019) Assessment of DNA topoisomerase i unwinding activity, radical scavenging capacity, and inhibition of breast cancer cell viability of N-alkyl-acridones and n, N′-dialkyl-9 9′-biacridylidenes, *Biomolecules*, **9**, 177.
38. Hridya,V., Hynes,J.T. and Mukherjee,A. (2019) Dynamical recrossing in the intercalation process of the anticancer agent proflavine into DNA. *J. Phys. Chem. B*, **123**, 10904–10914.
39. Prasher,P. and Sharma,M. (2018) Medicinal chemistry of acridine and its analogues. *MedChemComm*, **9**, 1589–1618.
40. Laskowski,T., Andrałojć,W., Grynda,J., Gwarda,P., Mazerski,J. and Gdaniec,Z. (2020) A strong preference for the TA/TA dinucleotide step discovered for an acridine-based, potent antitumor dsDNA intercalator, C-1305: NMR-driven structural and sequence-specificity studies. *Sci. Rep.*, **10**, 11697.
41. Kuzuya,A. and Komiyama,M. (2000) Sequence-selective RNA scission by non-covalent combination of acridine-tethered DNA and lanthanide (III) ion. *Chem. Lett.*, **29**, 1378–1379.
42. Shi,Y., Machida,K., Kuzuya,A. and Komiyama,M. (2005) Design of phosphoramidite monomer for optimal incorporation of functional intercalator to main chain of oligonucleotide. *Bioconjugate Chem.,***16**, 306–311.
43. Kuzuya,A., Machida,K., Shi,Y., Tanaka,K. and Komiyama,M. (2017) Site-Selective RNA activation by acridine-modified oligodeoxynucleotides in metal-ion catalyzed hydrolysis: a comprehensive study. *ACS Omega*, **2**, 5370–5377.
44. Agard,N.J., Prescher,J.A. and Bertozzi,C.R. (2004) A strain-promoted [3+ 2] azide− alkyne cycloaddition for covalent

modification of biomolecules in living systems. *J. Am Chem. Soc.*, **126**, 15046–15047.
45. Jewett,J.C. and Bertozzi,C.R. (2010) Cu-free click cycloaddition reactions in chemical biology. *Chem. Soc. Rev.*, **39**, 1272–1279.
46. Krell,K., Harijan,D., Ganz,D.e., Doll,L. and Wagenknecht,H.-A. (2020) Postsynthetic modifications of DNA and RNA by means of copper-free cycloadditions as bioorthogonal reactions. *Bioconjugate Chem.,***31**, 990–1011.
47. Kim,E. and Koo,H. (2019) Biomedical applications of copper-free click chemistry: in vitro, in vivo, and ex vivo. *Chem. Sci.*, **10**, 7835–7851.
48. Fantoni,N.Z., El-Sagheer,A.H. and Brown,T. (2021) A hitchhiker's guide to click-chemistry with nucleic acids. *Chem. Rev.*, **121**, 7122–7154.
49. Muller,D., Zeltser,I., Bitan,G. and Gilon,C. (1997) Building units for N-Backbone cyclic peptides. 3. Synthesis of protected Nα-(ω-Aminoalkyl)amino acids and Nα- (ω-Carboxyalkyl)amino acids. *J. Org. Chem.*, **62**, 411–416.
50. Romuald,C., Busseron,E. and Coutrot,F. (2010) Very contracted to extended co-conformations with or without oscillations in two- and three-station [c2]daisy chains. *J. Org. Chem.*, **75**, 6516–6531.
51. Hickey,S.M., Ashton,T.D., Khosa,S.K. and Pfeffer,F.M. (2012) An optimised synthesis of 2-[2,3-Bis (tert-butoxycarbonyl)guanidino]ethylamine. *Synlett*, **23**, 1779–1782.
52. Asseline,U., Delarue,M., Lancelot,G., Toulmé,F., Thuong,N.T., Montenay-Garestier,T. and Hélène,C. (1984) Nucleic acid-binding molecules with high affinity and base sequence specificity: intercalating agents covalently linked to oligodeoxynucleotides. *Proc. Natl. Acad. Sci. U.S.A.*, **81**, 3297–3301.
53. Babu,Y.R., Bhagavanraju,M., Reddy,G.D., Peters,G.J. and Prasad,V.V.S.R. (2014) Design and synthesis of quinazolinone tagged acridones as cytotoxic agents and their effects on EGFR tyrosine kinase. *Arch. Pharm.*, **347**, 624–634.
54. Le Gac,G. and Férec,C. (2005) The molecular genetics of haemochromatosis. *Eur. J. Hum. Genet.*, **13**, 1172–1185.
55. Hanson,E.H., Imperatore,G. and Burke,W. (2001) HFE gene and hereditary hemochromatosis: a HuGE review. *Am. J. Epidemiol.*, **154**, 193–206.
56. Asseline,U., Bonfils,E., Dupret,D. and Thuong,N.T.J.B.c. (1996) Synthesis and binding properties of oligonucleotides covalently linked to an acridine derivative: new study of the influence of the dye attachment site. *Bioconjugate Chem.,***7**, 369–379.
57. Rapireddy,S., He,G., Roy,S., Armitage,B.A. and Ly,D.H. (2007) Strand invasion of mixed-sequence B-DNA by acridine-linked, γ-peptide nucleic acid (γ-PNA). *J. Am Chem. Soc.*, **129**, 15596–15600.
58. Kim,H.-K., Kim,J.-M., Kim,S.K., Rodger,A. and Nordén,B. (1996) Interactions of intercalative and minor groove binding ligands with triplex poly (dA)⊙[Poly (dT)] 2 and with duplex poly (dA)⊙ poly (dT) and poly [d (AT)] 2 studied by CD, LD, and normal absorption. *Biochem.*, **35**, 1187–1194.
59. Wu,M., Wu,W., Gao,X., Lin,X. and Xie,Z. (2008) Synthesis of a novel fluorescent probe based on acridine skeleton used for sensitive determination of DNA. *Talanta*, **75**, 995–1001.
60. Finlay,G.J., Riou,J.F. and Baguley,B.C. (1996) From amsacrine to DACA (N-[2- (dimethylamino)ethyl]acridine-4-carboxamide): selectivity for topoisomerases i and II among acridine derivatives. *Eur. J. Cancer*, **32a**, 708–714.
61. Adams,A. (2002) Crystal structures of acridines complexed with nucleic acids. *Curr. Med. Chem.*, **9**, 1667–1675.
62. Hoory,E., Budassi,J., Pfeffer,E., Cho,N., Thalappillil,J., Andersen,J., Rafailovich,M. and Sokolov,J. (2017) Discrimination of adsorbed double-stranded and single-stranded DNA molecules on surfaces by fluorescence emission spectroscopy using acridine orange dye. *J. Fluoresc.*, **27**, 2153–2158